SPACE-BORNE CORONAGRAPHY

Dedicated to: B. Lyot, who built the first ground-based coronagraph; G. Newkirk, who built the first flying coronagraph; G. Nikolsky, who built the largest, each of whom prematurely passed away.

SERGE KOUTCHMY*

NRC Resident Associate at AFGL/NSO/Sacramento Peak Observatory, Sunspot, New Mexico 88349, U.S.A.

(Received 15 February, 1988)

Abstract. We consider the main aspects of a rather delicate discipline, space-borne coronagraphy, which is essentially performed with white-light, externally-occulted coronagraphs. Methods of observation and recent results are presented in a scientific section; a short account of historical rocket-borne and balloon-borne experiments is also given. The review concentrates on both the NRL-type coronagraphs and the HAO-type coronagraphs, stressing the essential features and merits of numerous experiments which were flown. A small section is devoted to other designs. A large number of figures, including many drawings, are used to illustrate the growing complexity of experiments.

Table of Contents

* On leave from Paris Institut d'Astrophysique CNRS, 98 Bis Bd Arago, F-75014, Paris, France.

Space Science Reviews **47** (1988) 95–143.

1. Introduction

The solar corona is the most extended, optically thin part of the solar atmosphere, which is essentially made up of a hot fully-ionized and magnetized plasma in a dynamical state. Its study is of general interest for both the physicist and the astronomer, and all stars seem to show evidence for a corona. Stellar coronae can be of plasma origin, as a coronal extension of the stellar chromosphere, producing a significant amount of X-ray emission, or of dust origin, presumably coming from the proto-star cloud emitting in infra-red. This second component exists also around the Sun (the F-corona), but its origin is not yet well established (see further). Additionally, the analysis of solar coronal data is of fundamental interest in developing models for solar-terrestrial relationships, including the prediction of geophysical effects. Recurrent geomagnetic disturbances are related to coronal holes and the so-called 'fast wind'; sudden large disturbances are connected with solar flares taking place at the coronal level. Therefore, the solar corona is becoming more and more interesting for geophysicists.

In the past and still today, the solar corona is observed during total solar eclipses. Then, the Earth's atmosphere is sufficiently dark, provided the observer is located inside the shadow of the Moon, to show, by contrast, the extended atmosphere around the Sun. During these short, transient, and rare events, the corona is studied in great detail with instruments brought up to the eclipse site. The limitations of these observations is quite obvious: only a very short time available to perform the observations; no temporal coverage of the dynamical phenomena; etc. To overcome these limitations, a new instrument was invented by B. Lyot in 1930, the coronagraph (see Billings, 1966; Dollfus, 1983). Unfortunately, the coronagraph used in a ground-based observatory is fundamentally limited by the day-time brightness of the Earth's atmosphere, even in a high-altitude observatory (see Figure 1). So ground-based coronal observations are essentially limited to the study of the inner corona in emission lines. To measure the electron corona, a so-called '*K*-coronameter' is used to extract the *pB*-values, where *p* is the linear polarization rate; here again, the Earth's atmosphere limits severely the quality of the observations and consequently, the achieved spatial resolution.

With the advance of space technology, it has become possible to overcome the large limitations imposed by the Earth's atmosphere. However, when the level of the sky background is decreased drastically, the instrumentally scattered light coming from the direct illumination of the main objective produces a relatively large amount of light (see Figure 1), masking the most interesting parts of the corona. Therefore, all space-borne

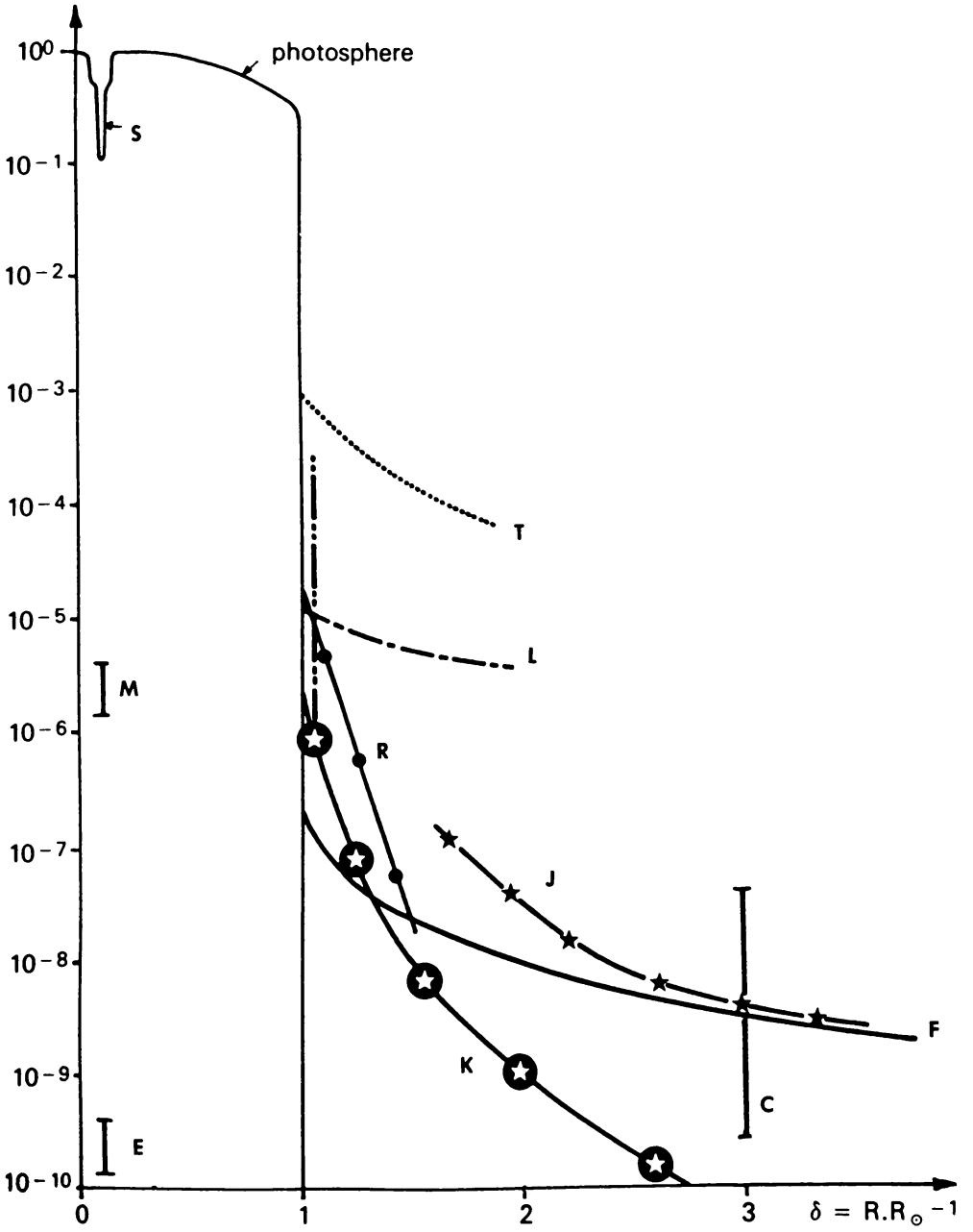

Fig. 1. Radial variation of different levels of intensity met in coronal studies. R is the solar radii; S corresponds to the intensity profile of a sunspot; T is the typical intensity profile of the aureola at the sea level; and L is the level of the instrumentally of origin background at 500 nm, in a coronagraph operating in a good high altitude site. R is the radial white-light intensity profile of a coronal enhancement; K is the same for the background electron corona; and J for a large streamer. C corresponds to the sky levels measured during solar total eclipses. M is the level corresponding to a full Moon and E to the earthshine.

coronagraphs operating in white-light use a design originally introduced by Evans (1948), together with the Lyot (1939) optical scheme. This design is called 'external occultation', as it uses a device external to the main objective to produce a shadow (the Sun is artificially eclipsed) and considerably reduces the amount of instrumentally scattered solar light (see further).

By operating outside the Earth atmosphere it has also been possible to extend the observations to the X–EUV spectral regions, where the corona can be observed without disturbances from the solar disk. The same is true when a radio telescope is used. However, the technology and the methods of analysis are definitely different from that which is used with white-light coronagraphs, although these methods are complementary. So we will concentrate here only on the description of white-light, externally occulted coronagraphs and their application in space.

2. Scientific Objectives

Our knowledge on the solar corona (see, e.g., Billings, 1966; Hundhausen, 1972; Zirker, 1977) has been reviewed in several recently published international conferences, e.g., Marsden (1986), Poland (1986), Altrock (1987), *The Hydromagnetics of the Sun* (ESA SP-220), and *Coronographie d'ici à l'an 2000*, Bougeret (ed.), CNRS, 1988. Good recent reviews can be found in Zirker (1985, 1987), Rosner (1986), Schwenn (1986), and Pneuman (1986). Accordingly, there is no need to review again this subject here as no essential results were obtained last year. Let us briefly address the subject and try to stress the new problems to be treated with coronagraphs.

Fig. 2. Image of the solar corona enhanced to show the overlapping structures. Processed solar total eclipse picture obtained on June 30, 1973 (Paris Institut d'Astrophysique, CNRS). The Moon-disk has been replaced on this composite with the Hα image of the Sun observed simultaneously at Sacramento Peak Observatory.

2.1. THE CORONAL STRUCTURES

Figure 2 represents a modern view of the solar coronal structures as revealed on an eclipse picture of good resolution taken near the sunspot minimum of activity. The effect of the overlap of different optically thin structures integrated along the line-of-sight is particularly clear in this white-light photo. A comprehensive presentation of these structures can be found in Koutchmy (1977). White-light observations of the corona permit a precise and straightforward determination of the electron densities, provided the geometrical parameters (cross sections; orientation; positions; etc.) of the structures are known. We then meet the first fundamental difficulties of coronal physics that spaceborne coronagraphs have attempted to resolve: what is the actual extension of the structures? What are their shapes? Is a streamer a sheet, a bubble-like feature, or an arcade? A long standing controversy still exists when arch-like or loop-like large-scale structures are observed, as they often can be equally considered as a three-dimensional

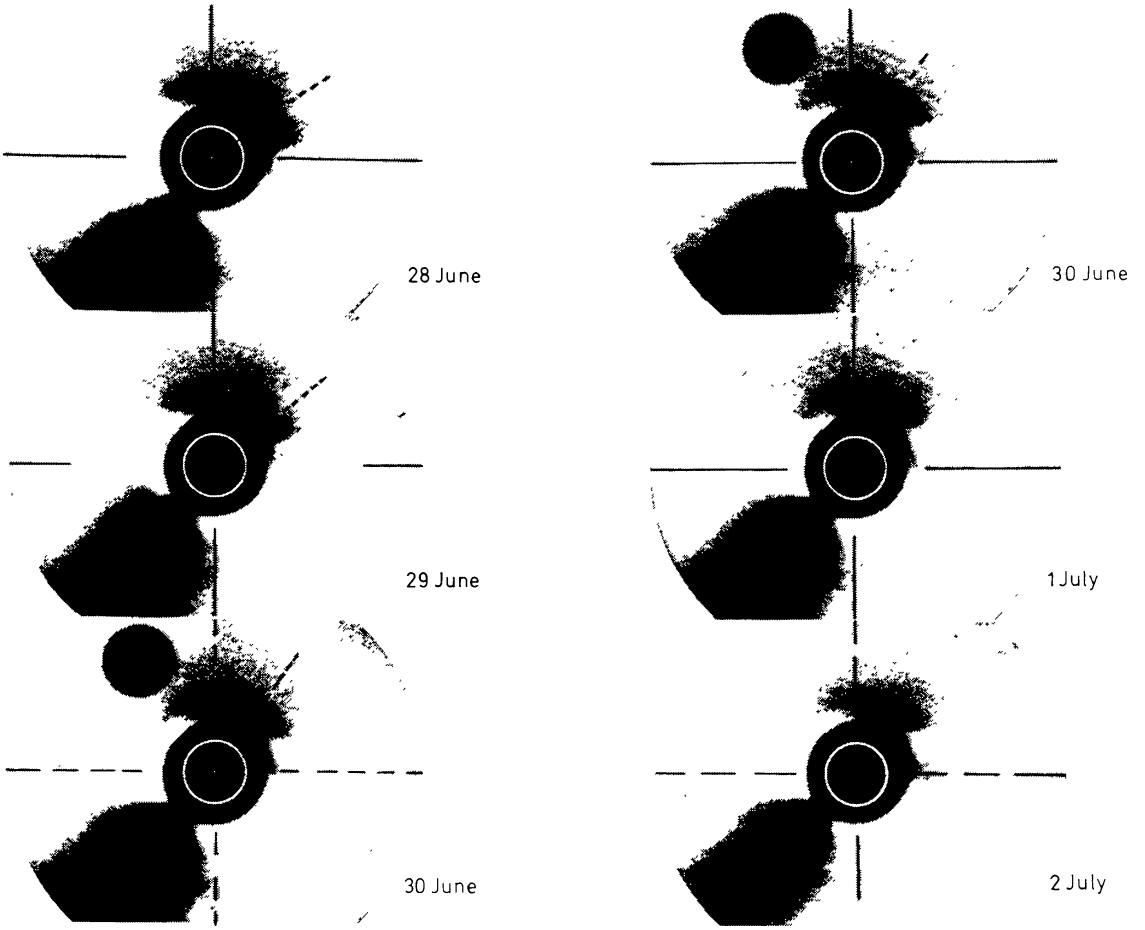

Fig. 3. Mosaic of coronal pictures prepared using few of the ATM–HAO coronagraph pictures collected during the SkyLab missions in 1973. The rotation of the large-scale coronal structure can be easily followed from day to day, although intrinsic variations cannot be ruled out. The inner part of the corona is masked by the external occultation, but the true size of the solar disk has been drawn up; note also the position of the shadow produced by the pylon supporting the external occulters at the bottom left. The picture taken on June 30, 1973 shows the moon disk projected on the corona, as a solar total eclipse was in progress (see Figure 2).

bubble or as a cloud-like structure. An equally confused situation exists concerning the morphological particularity of coronal hole regions: are the polar jets or plumes actually coming from these regions, or are they only a part of the edges or even ends of streamers surrounding the hole, viewed on projection?

One of the most promising methods to be used for resolving these questions, which are intimately connected with physical problems of the corona, is to try to get a stereoscopic view of the corona. For this, we can take advantage of the rotation of the structures together with the underlying chromosphere, as evidenced in Figure 3. However, proper variations of the structures cannot be ruled out and, indeed, are largely evidenced in the case of a transient phenomena like a coronal mass ejection (C.M.E.) (see Wagner, 1984). Another aspect of the study of coronal morphology and the corresponding density structures is the inferred amplitude and distribution of the magnetic field imbedded in the structures and clearly dominating the gas pressure. Presumably, fine-scale structures need to be considered and a large improvement of the spatial resolution of coronagraphs is needed in future experiments. As far as the large structure is concerned, attempts made to compute the distribution of magnetic field lines, assuming potential fields, give mixed success when the computed maps are compared with the observed structures. For example, it is not clear at all how the magnetic field lines look around filaments or prominences; above coronal holes, a largely divergent and open magnetic field configuration is inferred, but awaits observational confirmation. Clearly, direct magnetic field measurements are needed.

2.2. Coronal heating and acceleration of the solar wind

We now consider the most current problems in solar coronal physics. They have been briefly reviewed in an unpublished formulation by Parker (1987) of the scientific perspectives of the proposal for a 'wide-field white-light and spectroscopic coronagraph for the SOHO spacecraft', produced by an international consortium lead by the Naval Research Laboratory (NRL) group. We will try to summarize the lines of Parker and follow his conclusions. Past observations show that the corona is in a dynamical state, with rapid energy release producing mass eruptions. There are also coronal holes undergoing continual outward expansion, but small-scale inward motion of cool material is also present. Finally, there are regions of intense field showing occasional burst and mass ejection at the location of solar flares. It seems that the causes of the activity are complex and lie at small scales. Concerning the source of solar wind, the origin could be the quiet corona (outside the active regions where field lines are closed, or at least too large in amplitude) and in coronal holes which are responsible for a continual outflow of gas. The expansion is presumably a consequence of the outward extension of the million degree coronal temperature maintained by thermal conduction and a powerful, but essentially unknown, heating mechanism. The energy input needed is typically 10^6 ergs cm^{-2} s^{-1}, essentially lost in the expansion of the gas. We notice that the source of the solar wind is not clearly known.

Conversely, in the active parts of the corona the magnetic field prevents the expansion into space. The gas density and temperature build up until the X–UV emissions balance

the energy input. Flares and CME's are produced by the shearing and the deformation of the field due to motions at photospheric level. However, the source of the heat is not known, for both coronal holes and active corona. Magneto-acoustic gravity waves have been proposed to dissipate and create the chromosphere and pure Alfvén waves in the corona. But observations impose strict limits on the amplitudes and, additionally, they do not dissipate effectively until resonance effects are considered. Parker (1972), has proposed that the tangential discontinuities could be privileged locations in the solar corona where dissipation could take place, thanks to 'rapid point connections' there, as a consequence of the motions of the footprints at the photospheric level. The situation in the coronal holes is quite different, because the magnetic field lines are open out into space, so the available energy should be contained in some propagating waves; but it is not clear that waves alone account for the heat input. Small magnetic loops may be emitted continuously through the coronal hole, heating the gas and giving an outward momentum (see Pneuman, 1986). This is also suggested by the interpretation of *in situ* measurements taken at 1 AU. From these measurements, it seems that the solar wind should be regarded as a two-state phenomenon, the source of the slow wind being unclear. It is quite obvious that to answer this question, only coronagraphic observations can be of help, especially in the first few solar radii above the surface of the Sun, where the acceleration moves the gas up to supersonic speeds and where most of the thermal energy is consumed.

Many more questions can be addressed as far as coronal evolution is concerned: what is the effect of the emerging magnetic flux? What is the radial divergence of the coronal magnetic field? What physical processes are responsible for coronal evolution? How

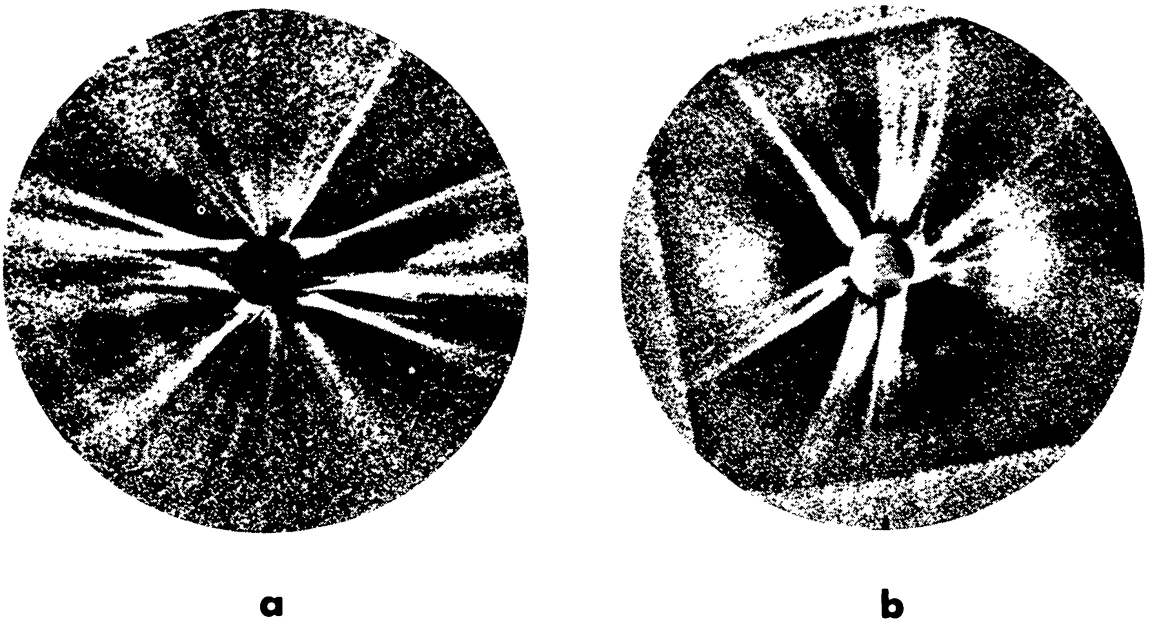

Fig. 4. Large-scale picture of the eclipse solar corona observed near the sunspot minimum of activity, in (a) (June 30, 1973) and near the sunspot maximum of activity in (b) (March 7, 1970). The central disk replacing the Moon disk has a radius of 1.3 solar radii so regions up to 12 solar radii are shown. In both pictures the North Pole is at the top (courtesy of Ch. Keller, Los Alamos Lab.).

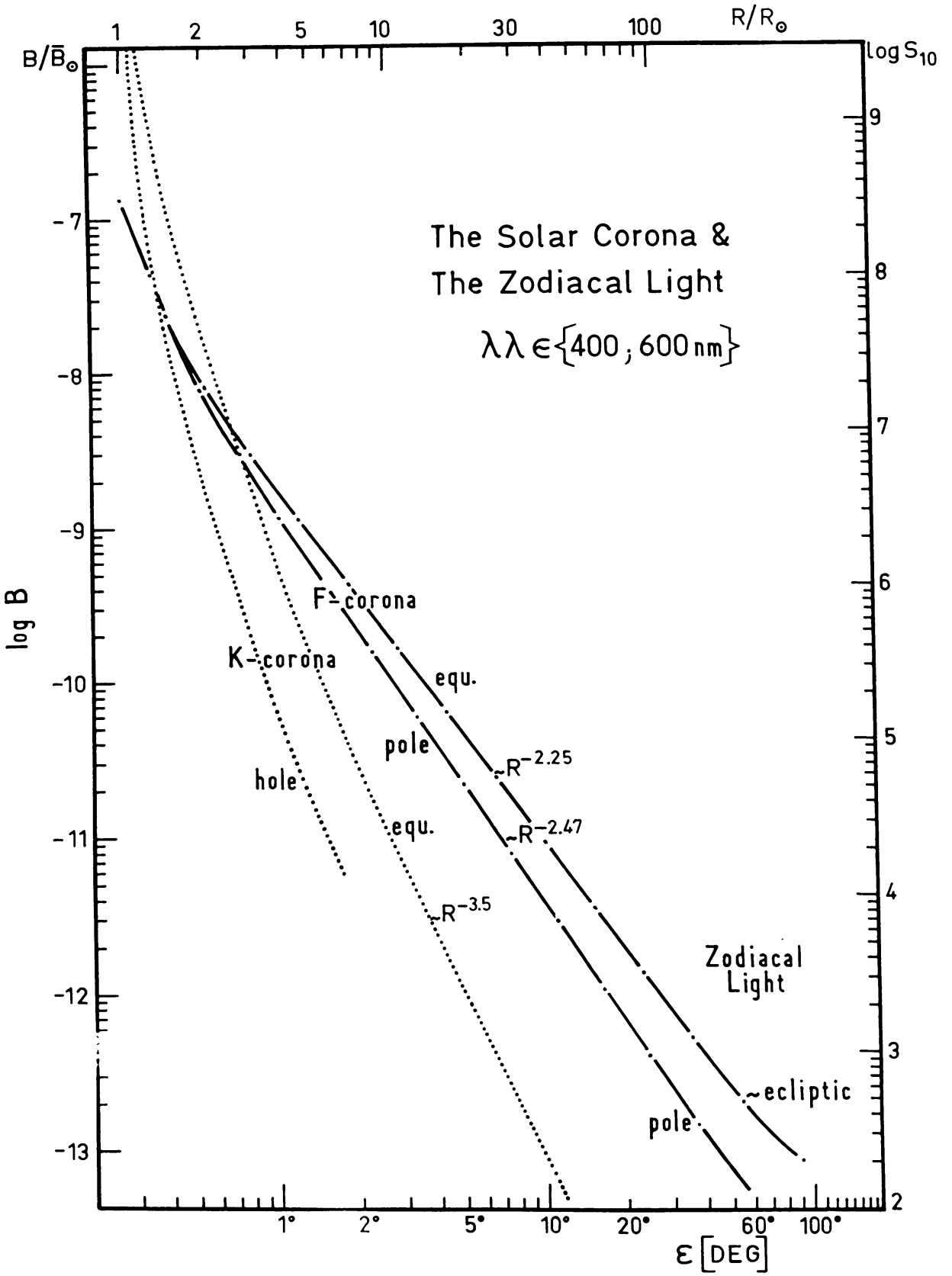

Fig. 5. Radial variation of the average intensities of the different components of the solar corona: *K* is the plasma corona and *F* the dust corona (from Koutchmy and Lamy, 1985).

does the CME evolve as it moves into the heliosphere? Large-scale eclipse pictures of the corona suggest also that the external regions, where the plasma is presumably accelerated at super-Alfvénic speed, are locations where important phenomena seem to occur (see Figure 4), including transient phenomena which apparently are not connected with surface phenomena. New generation space-borne coronagraphs with improved resolution will certainly bring new light on this aspect of coronal dynamics.

2.3. The dust corona

At a distance of approximately two radii from the Sun center, the dust component of the solar corona starts to dominate the white-light radiation coming from the electron corona (see Figure 5). The light is produced by the scattering on dust particles, of the same origin as for the zodiacal cloud (shown in Figure 6). Consequently, it is necessary to distinguish carefully between the *F*- and the *K*-component produced by the Thomson scattering on electrons. However, the study of the dust-corona is interesting in itself since, for example, its origin is still unknown (see Koutchmy and Lamy, 1985), as also

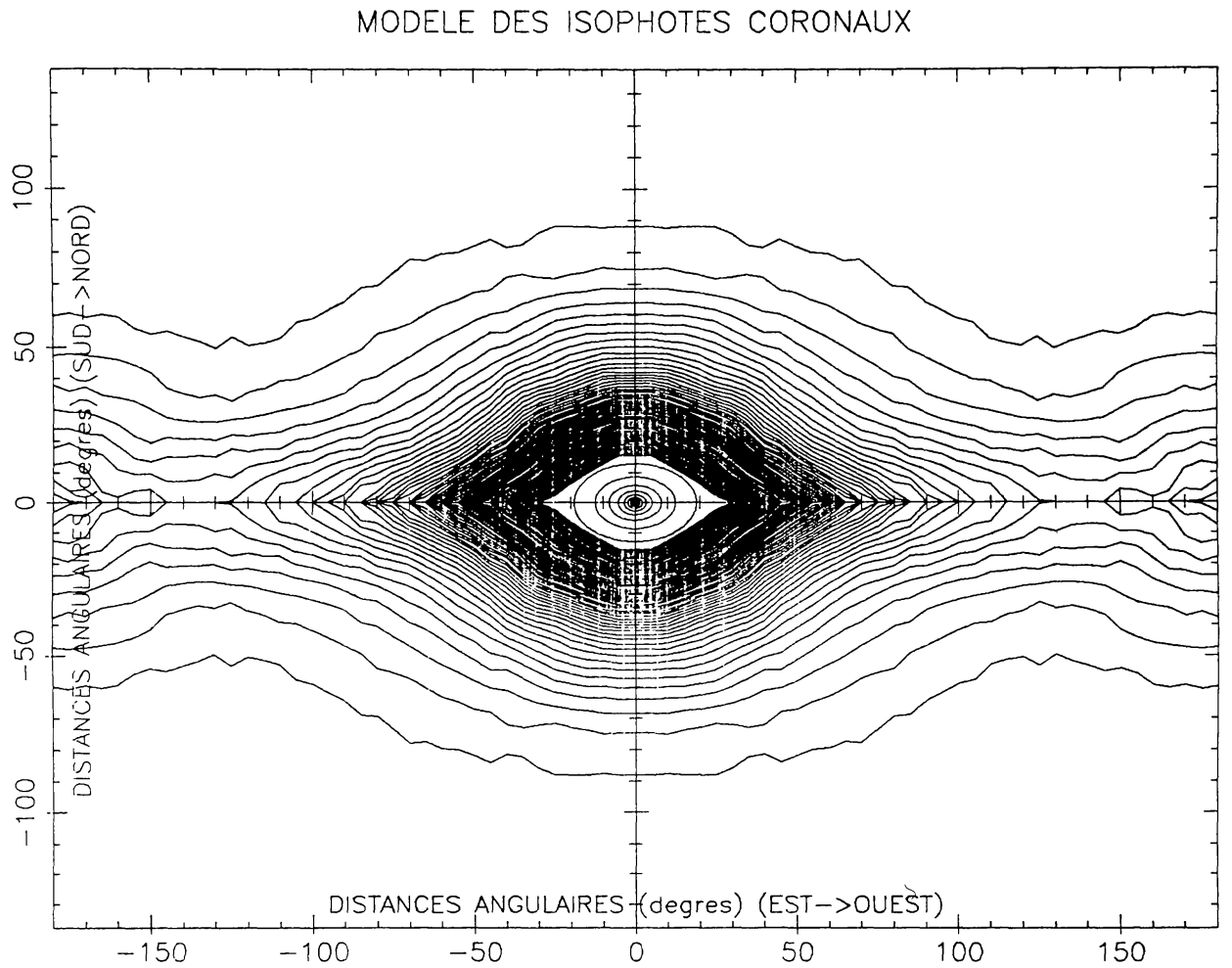

Fig. 6. The most external parts of the dust corona are elongated along the ecliptic and constitute indeed the zodiacal light as shown by the distribution of the coronal isophotes projected on a map with ecliptic coordinates; see Figure 5 to identify the isophotes (courtesy of Ch. Nitschelm, Paris Institut d'Astrophysique, CNRS).

is the origin of the zodiacal light, its interplanetary counterpart. The most relevant information concerning the *F*-corona is awaiting precise measurements of its color, including the infra-red part of the spectrum, as a thermal emission is most likely to occur. The near-Sun part of the dust corona being heated by solar radiation, its proper emission can be observed. Because of the UV irradiation of the dust particles and also because the sputtering is probably efficient, a 'cavity' region around the Sun, or dust-free zone, could exist. Rings have even been suggested around the Sun, at distances near four radii and further. The most interesting observation performed recently with the SOLWIND coronagraph (see, e.g., Michels *et al.*, 1982), has been the discovery of Sun-grazing comets impacting the Sun. White-light coronagraphs are particularly well-suited to record these phenomena, and will also serve in the future as pilot instruments to alert other instrumentalist-observers equipped with spectroscopic capabilities for analyzing the processes occurring before and during the impact. A whole domain of dust-plasma interaction physics is opening up for future investigation and there again stellar astronomers will learn some important physics which probably plays a fundamental role in stellar systems.

3. The Externally Occulted Coronagraph and a Few Specific Optical Problems

Putting an external device before an optical system, to occult the solar disk, induces a few rather specific problems which have been rather seldom described in the literature. We will now review the main aspects of these problems, referring for more details to the papers of Purcell and Koomen (1962), Newkirk and Bohlin (1963), Fort *et al.* (1978), Lensky (1977, 1981), Smartt (1979), and Koutchmy and Belmahdi (1988). Very useful information can also be found in collective works contained in several proposals and experiment handbooks concerning coronagraphs (see further Sections 4 and 5).

3.1. The external occultation and the problem of apodization

Externally occulted space-borne coronagraphs have been progressively improved to reduce the residual level of instrumentally scattered light, based on the design originally introduced by B. Lyot. The 'sky-photometer', originally designed by Evans (1948), used a single disk to produce a slight external occultation of the objective lens. Furthermore, the level of scattered light behind the disk was successively lowered, using different designs: toothed disk or wheel by Purcell and Koomen (1962) (see Figure 7), or two disks (presumably designed to eliminate a theoretically predicted bright point produced behind the first disk when a point-like source is used) or better, a *three-disk occulter* by Newkirk and Bohlin (1963). A system with 170 disks was also envisaged by Newkirk and Bohlin; however, the most successful space-borne coronagraphs, flown aboard Skylab, SMM and P-78 (see further), all used 3-disk systems, although the improved toothed disk was shown to give, under special circumstances, even better results (see Fort *et al.*, 1978). Finally, in the last few years a more complicated rotating system, with a sector-like entrance aperture, was developed to study the outer extremes of the solar corona equivalent to levels $10^{-11}\,B_{\odot}$. A theoretical treatment, showing the last system

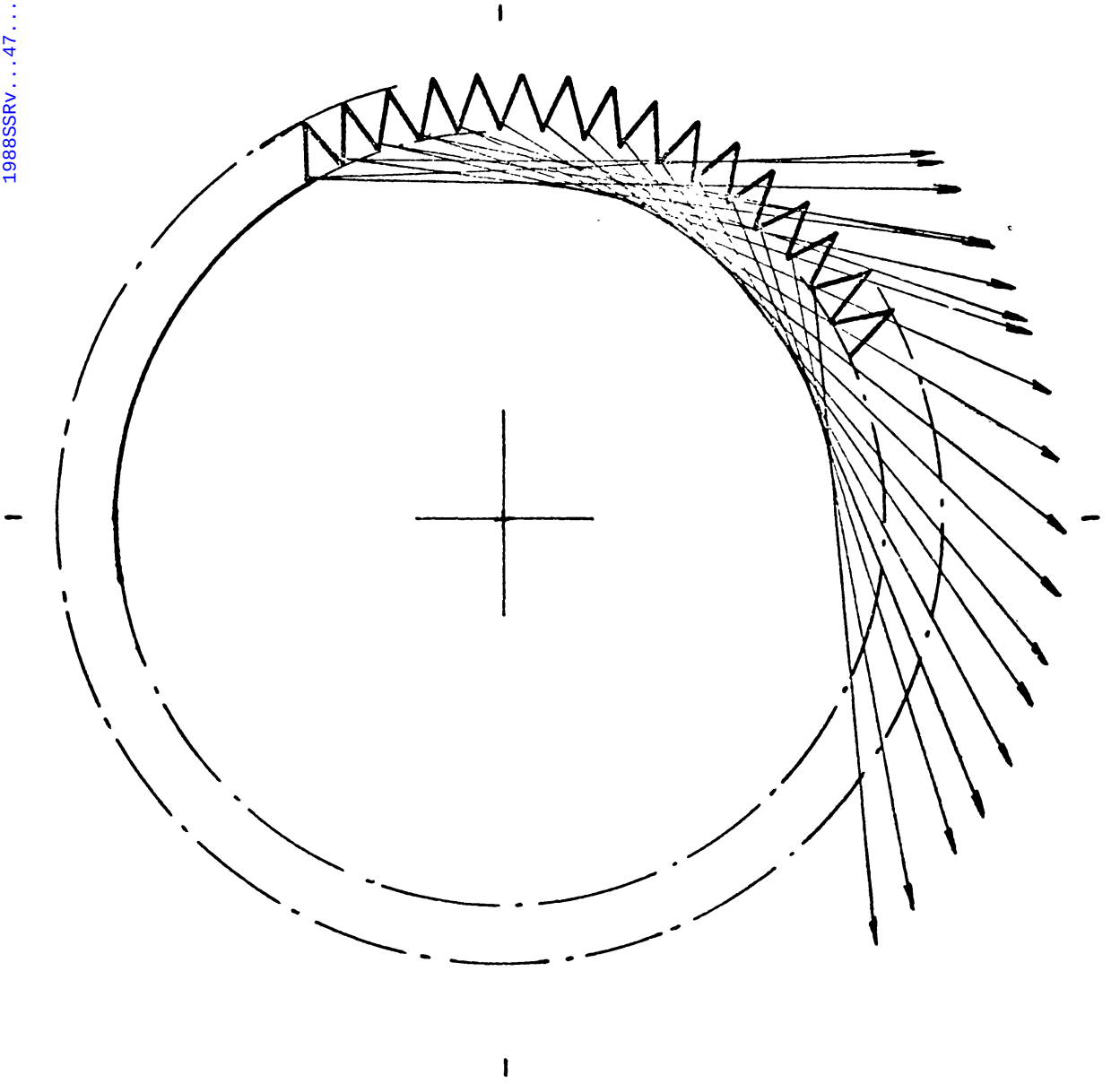

Fig. 7. Direction of diffracted parallel light from the periphery of a sawtooth disk or serrated edge (from Purcell and Koomen, 1962). The incident beam is perpendicular to the plane of the figure and the directions of the diffracted rays are shown in projection on the plane of the figure, so they do not reach the optical system of a coronagraph.

to be the best, has been published recently by Lensky (1981) and subsequent papers (in Russian). Taking into account all theoretical and experimental results published, Koutchmy and Belmahdi (1988) repeated the analysis of Newkirk and Bohlin (1962) and Fort *et al.* (1977), with the aim of reconsidering an external occulting system that could achieve a still lower level of scattered light over the main objective lens and that, presumably, will reduce the constraints imposed over the whole coronagraphic optical system. Let us now enter a few theoretical considerations: formulae giving the amount of scattered light near the optical axis at a distance L behind a *single disk* of radius r, illuminated by the solar disk of angular radius $R_\odot$ (taken equal to 4.65×10^{-3} rad) at

a wavelength λ, neglecting the center-to-limb variation, have been derived using different methods. Here, for convenience we essentially rewrite these formulae using the same practical notations. The amount of scattered light $s(r, L, \lambda)$, is considered near the optical axis, behind the occulter, in units of the average solar luminosity $\bar{I}_\odot$. In the case of a single disk, the Fort *et al.* (1978) formula (9) is rewritten as:

$$S_1^F(r, L, \lambda) = \left[\pi^2 R_\odot \left(1 - \frac{R_\odot L}{r}\right)\right]^{-1} \frac{\lambda}{r} . \tag{1}$$

Similarly, the formula (6) of Lensky (1981) is rewritten as

$$S_1^L(r, L, \lambda) = \left\{\pi^2 R_\odot \left[1 - \left(\frac{R_\odot L}{r}\right)^2\right]\right\}^{-1} \frac{\lambda}{r} . \tag{2}$$

Note that $S_1^F = S_1^L$ only when $r = R_\odot L$, which is unlikely to be the case in practice, due, for example, to alignment errors. The discrepancy appearing when S_1^F and S_1^L are compared originates the approximation made by the authors; numerical results show a satisfactory agreement for the order-of-magnitude estimations (see Table I), the

TABLE I

Theoretical and measured levels of scattered light near the optical axis behind different occulting systems (in units of the average intensity of the solar disk)

Authors	System	Level	Remarks
Fort *et al.*, 1978 [4]	Single disk (theor.)	2.245×10^{-3}	(1) (2)
Lensky, 1981 [5]	Single disk (theor.)	1.733×10^{-3}	(1)
Koutchmy *et al.*, 1988	Single disk (exp.)	1.33×10^{-3}	(1)
Fort *et al.*, 1978 [4]	Toothed disk (exp.)	1.497×10^{-4}	(1) (3)
Koutchmy *et al.*, 1988	Toothed disk (exp.)	1.01×10^{-4}	(1)
Lensky, 1981 [5]	2-disk system (theor.)	8.96×10^{-5}	(4)
Lensky, 1981 [5]	3-disk system (theor.)	2.25×10^{-5}	(5)
Koutchmy *et al.*, 1968	Multi-thread system (exp.)	8.0×10^{-6}	(1)

(1) All calculations and measurements reported are with a solar source and an occulter of $r = 7.5$ mm radius (backside) situated at a distance $L = 450$ mm of the primary lens; $\lambda = 550$ mm (green region).
(2) The level given by these authors corresponds to the level averaged over the area near the optical axis.
(3) Taking into account the factor 15 of reduction given by these authors.
(4) Assuming (1) for the last disk and $\Delta r/\Delta L = 0.010$, $\Delta r = 0.2$ mm, see formula (3).
(5) A factor of 4 reduction with respect to (4).

difference being on the order of the differences between calculated values and the experimentally measured values by Koutchmy and Belmahdi (1988). The situation is far more complicated when toothed disks and multiple disk occulters are considered; only Lensky (1981) gave formulae introducing new parameters. In the case of a *toothed disk*, the outer and inner diameters, the apex angle, and the number of teeth are taken into account, making the formula complicated. However, Fort *et al.* (1978) have shown

experimentally that the quality of the *polishing* of the teeth plays the most important role in determining S, and they achieve a reduction in the amount of a scattered light near the optical axis by a factor of 15 less than that predicted by the theoretical S_1^F results. In the case of a 2-disk system, we rewrite the formula (8) of Lensky for practical use, assuming that the last disk, situated closest to the objective lens, has a radius r; the preceding one, situated at a distance ΔL from it, has a radius $r + \Delta r$. The amount of scattered light is then equal to:

$$E_2^L = \left\{4\pi^4 R_\odot \left[1 - \left(\frac{R_\odot}{\Delta r}\,\Delta L\right)^2\right] \frac{\Delta r}{\Delta L}\left(1 - \frac{\Delta r}{\Delta L}\,\frac{L}{r}\right)^2\right\}^{-1} \frac{\lambda^2}{\Delta r r}\,. \tag{3}$$

As observed by Lenskii, the formula degenerates for $\Delta r/\Delta L = R_\odot$ or $\Delta r/\Delta L = r/L$. Practically, this is never the case, since $R_\odot < \Delta r/\Delta L < r/L$. The value calculated in our case using formula (3) is entered in Table I; we point out that perfect alignment is assumed. Finally, for the case of a 3-disk system (the most commonly used so far for space-borne coronagraphs), Lensky did not perform a detailed calculation, but discussed the case from theoretical considerations, predicting that a reduction by a factor of 4 could be achieved. The corresponding value was also entered, although the measurements of Koutchmy and Belmahdi (1988), did not succeed in showing such a low level with this system. These measurements were performed under laboratory conditions at Paris Institut d'Astrophysique, CNRS, using an artificial source simulating the color and the extension of the Sun, superposed on a 'dark' background. The results for different occulting systems are given in Table I; typical values are entered; they depend critically on the quality of alignment of the occulter, held by a support with 5 deg of freedom. Measurements are well-reproducible; the quality of the alignment can be checked visually and photographs of the bright fringes were produced (see Figure 8). The parameters used for these measurements correspond to the geometrical configuration of a rather compact externally-occulted coronagraph. The scattered light level was measured at a distance of 450 mm behind the back face of the occulters of diameter 15 mm, providing a comfortable over-occultation. All results of calculations entered in Table I are deduced using these parameters. Note that the effective wavelength corresponds to green. Surprisingly, the bright spot behind the single disk, seen in the work of Newkirk and Bohlin, was not recorded, presumably because the effect of a finite angle, for a solar source, was underestimated by these authors. This made possible the practical comparison between the different occulting systems, by measuring the amount of light precisely on the optical axis, using the pinhole photometer with an effective entrance aperture of 0.65 mm. Outside the optical axis, the intensity of light corresponds to a rather flat distribution, with increasing intensities when bright fringes are viewed (see Figure 4). Single disk, 3-disk, toothed-disk systems, and a new one called a *multi-thread* system were tested. The multi-thread occulter, which gives the best results, was prepared using a cylinder of 15 mm diameter. Different shapes were tried, including what is named a 'screw-like' truncated cone. The number of threads was around 35, the length of the truncated cone being 20 mm (see Koutchmy and Belmahdi, 1988 for more

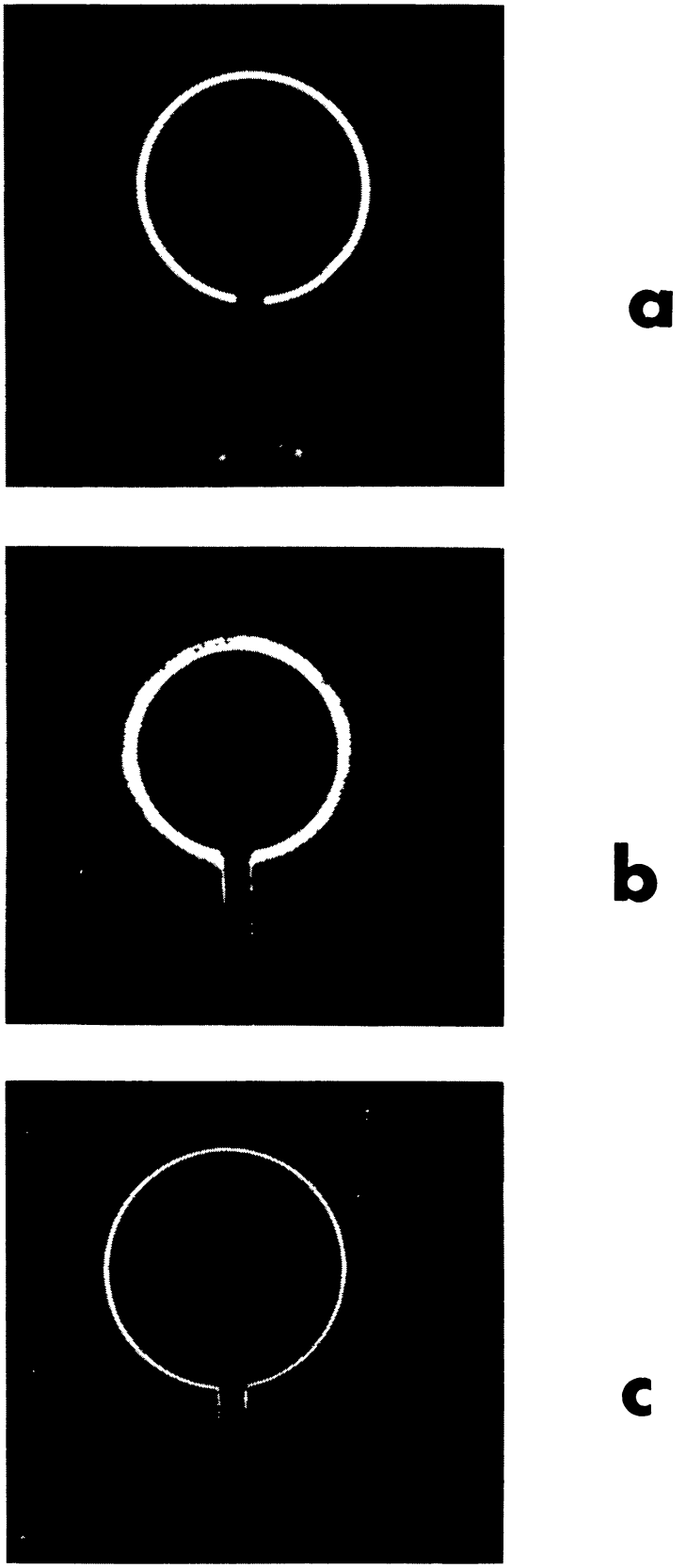

Fig. 8. Typical images of the diffraction fringes around different occulting system of: (a) single disk; (b) toothed disk; exposure time is increased by a factor of 7.5 with respect to image (a); (c) multi-thread occulter; exposure time as in (b) (from Koutchmy and Belmahdi, 1988).

details). Briefly, we conclude that the results given in Table I showed convincingly the superior quality of the multi-thread system, and should produce superior results in future coronagraphs.

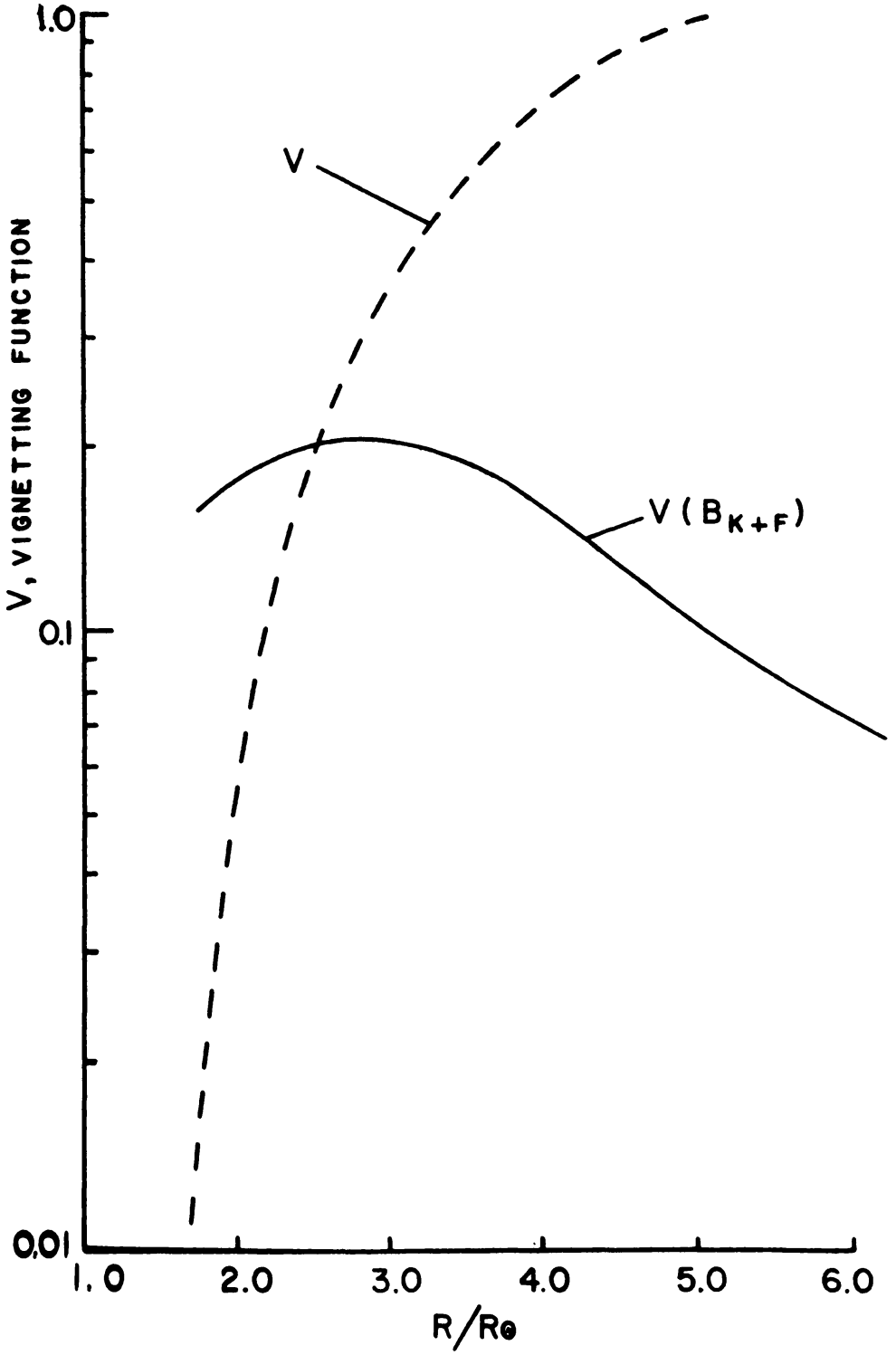

Fig. 9. The vignetting function measured on the ATM–HAO coronagraph operated on SkyLab in 73–74, V and the corresponding intensity distribution over the field of the detector produced by the coronal radiation, as a function of solar radii (from Csoeke-Poeckh *et al.*, 1977).

3.2. Problems of spatial resolution, vignetting, and absolute calibration

One of the problems inherent to an externally occulted system is the variable transmission over the field of view and the corresponding loss of spatial resolution. This effect is especially important for the most inner and unocculted parts of the corona. An additional effect is produced, further in the system, by the inner occulter used to suppress the bright parasitic fringes leaving around the external occulter. Note that alignments are very critical in such a system, and a modern coronagraph includes the capability of controlling and improving the alignments during the observations in space, at least at the level of the inner occulter (see Section 5.2). The vignetting effect produced

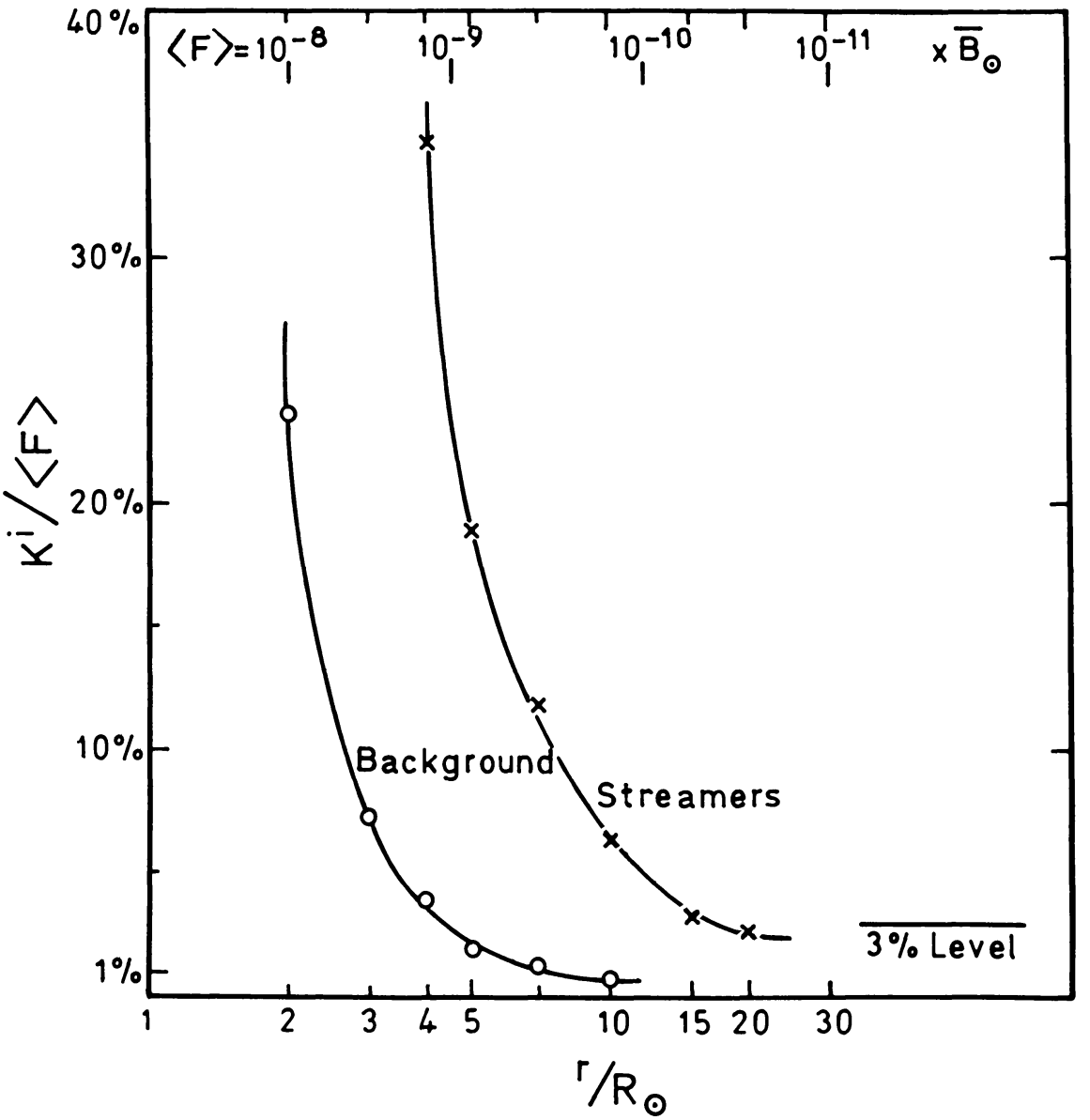

Fig. 10. Radial variation of the contrast ratio of the electron K-corona over the background dust F-corona for the case of a streamer situated in the plane of the sky and for the case of the background electron corona corresponding to a typical coronal hole region (see Figure 5).

by the external occulter is indeed a useful effect to reduce the dynamical range of intensities which has to be recorded with the detector (see Figures 1, 5, and 9). Accordingly, the effect should be calibrated accurately and, if possible, optimized to give a flatter field on the detector (see Figure 9). The effective modulation transfer function of the detector is finally affected by the intensity levels achieved through the signal-to-noise ratio, and this should be taken into consideration. However, the spatial resolution is already degraded in the inner parts of the corona by the partial occultation effect of the primary objective; this degradation is roughly proportional to the vignetting effect in the radial direction, so the effective resolution of an externally occulted coronagraph is always a function of the radial distance. Fortunately, the primary objective becomes fully illuminated when the external parts of the corona are considered and where the structures show a rather small contrast. Figure 10 gives the variation of the contrast as a function of radial distances for two typical cases. In the most favorable case of a coronal streamer, the contrast to be measured reaches values between 4 and 10% only for distances between 7 and 10 solar radii. In addition, the modulation becomes very small and can barely be detected without the use of special image processing methods. In the case of the background electron corona, the detection becomes difficult already at 4 solar radii and *polarization analysis* should be practiced. Indeed, at these distances and further, the electron corona is almost fully radially polarized, so its intensity can be extracted if the polarization ratio of the total intensity is precisely determined, assuming a negligible polarization ratio for the dust corona. This last assumption has not yet been checked with observations: this point is intimately connected with our knowledge of the local contribution of the dust in the overall F-corona intensity and needs further investigation.

More problems arise when one is willing to deduce reliable quantitative data. Then, not only relative response of the detector and the overall (both radial and azimuthal) transmission of the system should be known, but also the absolute response; accordingly, the stability in time of the detectors and the constancy of the transmission properties of the optical system should be controlled. A powerful method to get a reliable absolute calibration consists of observing stars crossing the field of view. Even the moon was used in the past (see, e.g., Csoeke-Poeckh *et al.*, 1977) to deduce a calibration of both the transmission of the coronagraph and of the measured intensities in absolute units, using the average levels of the earthshine during the transit over the field of view; additionally, this observation permits an estimation of the level of the parasitic instrumentally scattered light, because the corona is occulted by the moon during this partial exlipse. Observation of the planet Venus could also be used, but *stars* seem far more reliable, as their magnitude is well known and can be used as a 'stellar constant' (see Lebecq *et al.*, 1985). No doubt in the future a high photometric accuracy will be achieved with space-borne coronagraphs, thanks to the use of photometric detectors like the CCD cameras and stellar photometric standards (bright stars with $m_v \lesssim 6$).

Concerning the spatial resolution which should, in the future, undoubtedly be improved, longer instruments can be designed to avoid the partial occultation of the primary objective. In addition, achromatic designs are preferable. Already the most

recent space-borne (see Section 5.2.2) coronagraph uses a primary lens made of a doublet, which represents a large departure from the original Lyot design. A further improvement would be the use of a coronagraphic quality *mirror* as a primary objective (see Smartt, 1979). Such a design would radically improve the capability of a coronagraph and would probably open up a completely new era in coronagraphic studies. Today this possibility exists, at least for a small aperture instrument, thanks to the availability of super-polished mirrors of a pure silicon substrate (Schwenn, 1987).

4. Early Flying Coronagraphs

Before describing the most significant coronagraphic space-borne instruments, it is useful to place this presentation in a more prespective view, to describe the chronological order of the 'events' which laid out this already long story. We attempted to review this story in Table II, feeling that, although this relation is incomplete, it needs to be

TABLE II

Brief historical account of the development of W.L. spaceborne coronagraphs

1930	B. Lyot invents the inner occulted coronagraph to be used in high altitude sites.
1948	J. Evans invents the externally occulted solar aureola photometer.
1960	G. Newkirk and J. Eddy perform the first stratospheric balloon experiment at $\simeq 25$ km with a single disc externally occulted solar photometer.
1963	Thanks to a successful rocket flight, the NRL group (R. Tousey and coll.) obtains the first non-eclipse image of the outer corona with a small NRL photographic coronagraph using an external occulting disk with a serrated edge.
1963	First attempt to fly from Algeria a French rocket-borne UV coronagraph which uses a mirror as a primary objective. The program was later abandoned.
1964	Successful balloon experiment 'Coronascope II', by the HAO group (Bohlin and Newkirk) and first image of the middle corona using a 3-disk occulting system.
1965	First attempt to fly on the satellite OSO-2 the NRL coronagraph with a compact 3-disk occulting system.
1967	Successful balloon experiment for recording the IR dust corona (R. M. MacQueen) using a triple straight edge occulting system and a scanning IR photometer.
1967–68	Successful balloon experiments by the French group (Dollfus and coll.) for photographing the middle corona using near IR film and an external occulting disk with serrated edge.
1963–72	Successful rocket flights by the NRL group of a flight instrument consisting of two coronagraphs mounted side by side to avoid the shadow effect produced by the pylon.
1971–74	First day-to-day coronal recording obtained with the NRL satellite-borne-coronagraph equipped with an SEC Vidicon on OSO-7; first observation of a large flare-induced coronal mass ejection.
1973–74	Successful Skylab missions with the HAO white-light coronagraph on ATM. More than 35 000 calibrated photographic pictures of high quality have been returned.
1976	First successful flight of a rocket-borne Soviet coronagraph.
1978	Design of a new class of light externally occulted coronagraphs in response to the call for proposals of experiments to be flown on the 'out-of-ecliptic' spacecraft (I.S.P.M.).
1979–85	Long series of coronal observations performed with the NRL coronagraph mounted on the P-78–1 polar orbit defense satellite. Sun-grazing comets discovered.
1980	Start of observations with a new generation coronagraph aboard the SMM Spacecraft. In 1984, the coronagraph is successfully revived, thanks to a Repair Mission.
1987	Design of a cluster of 3 complex new spaceborne coronagraphs for operation at the Lagrangian point L_1 aboard the SOHO spacecraft.

published. Furthermore, the description of early experiments, especially those which failed, is not an easy task, and a selection effect is inevitable. We hope that this effect will not bring any prejudice.

4.1. Balloon-borne experiments

4.1.1. *The High Altitude Observatory (HAO) Balloon-Borne Coronagraphic Experiments*

The first coronagraph flying at stratospheric heights was conceived by Newkirk and Eddy (1962) and indeed failed to observe the solar corona but permitted the definition of several new instrumental features which were later on incorporated in a second generation balloon coronagraph, named coronascope II (see Newkirk and Bohlin, 1963, 1965), making possible the acquisition of a long series of balloon pictures of the corona.

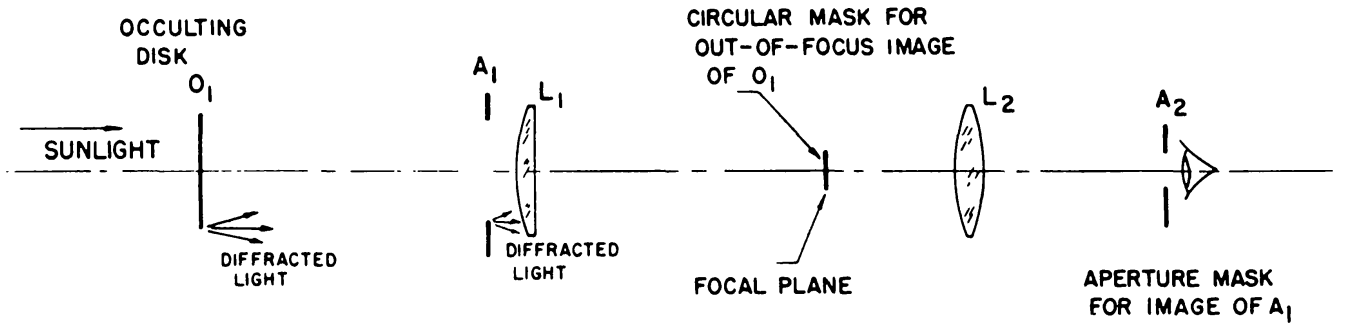

Fig. 11. Optical schematic of the first flying externally occulted coronagraph or photometer by Newkirk and Eddy (1962); note that the apodization of the external occulter was not perfect because the fringes produced by a single external disk are too bright and the Lyot coronagraph part was not conceived to reduce the light (scheme after Purcell and Koomen, 1962).

The initial scheme used is given in Figure 11. As Newkirk and Eddy stated, this instrument was made up of the adjunct of the Evans (1968) device to a conventional Lyot coronagraph and was not optimized for instrumentally scattered light. However, this first series of flights brought useful information on the earth atmospheric brightness at stratospheric heights, showing that it is necessary to go to infra-red in order to obtain a low enough sky background (nearly 10^{-9} of the average solar intensity at 850 nanometers and a 30 km height), in order to permit the observation of the corona at 2–6 solar radii (see Figures 1 and 5).

The more elaborate instrument successfully flown first in 5 March, 1964, is shown in Figure 12. For the first time, this instrument used the three-disk occulting system described by Newkirk and Bohlin (1963), which permitted the reduction of the light produced by the fringes which where diffracted by the first external disk (see Section 3.1). Photos of the corona obtained with infra-red films (at 830 nm effective wavelength) were calibrated during the flight, thanks to a specially designed photometer, providing photometric standards. Several large coronal streamers were observed and

1988SSRv...47...95K

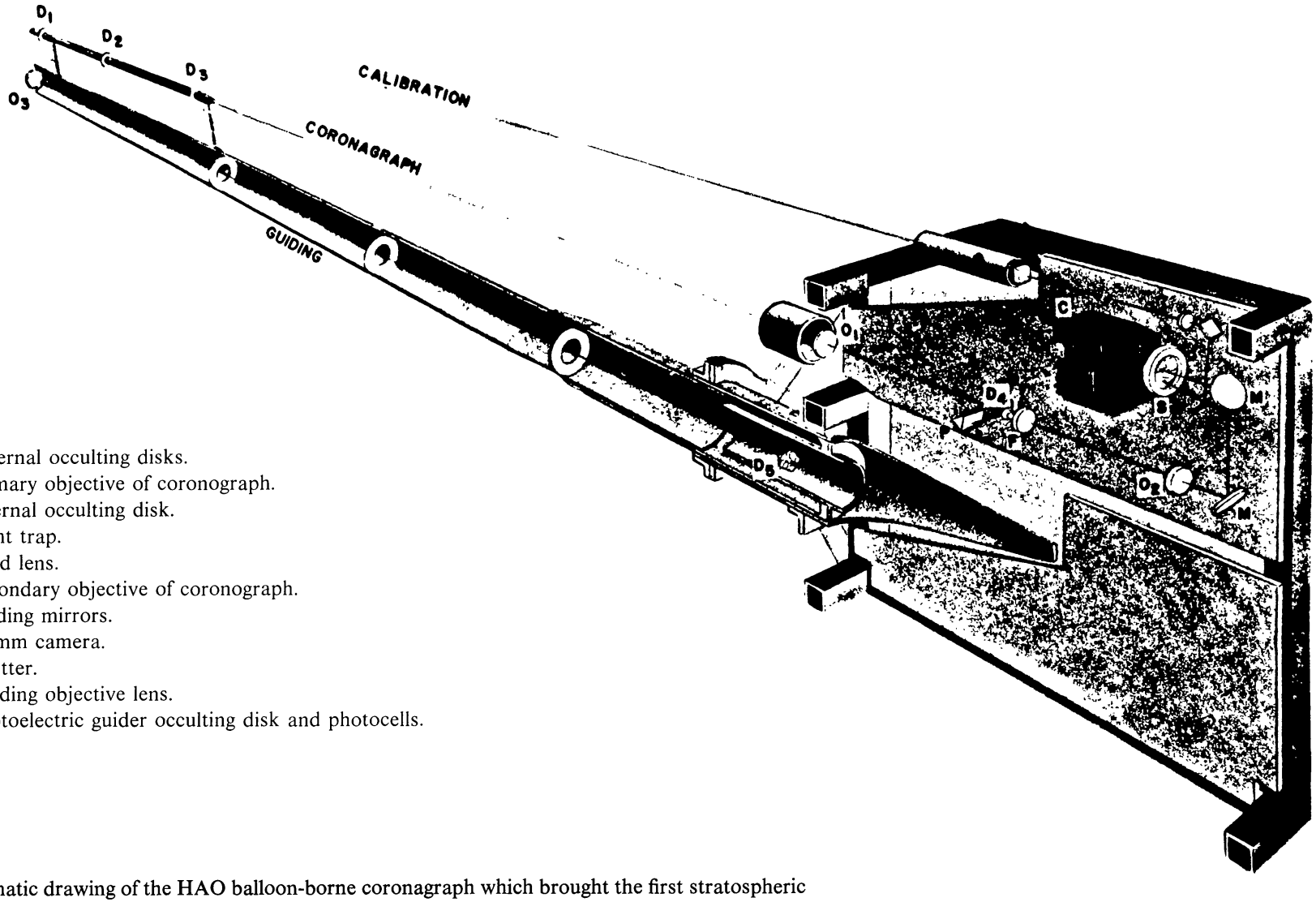

$D_1 - D_3$ – External occulting disks.
O_1 – Primary objective of coronograph.
D_4 – Internal occulting disk.
P – Light trap.
F – Field lens.
O_2 – Secondary objective of coronograph.
M – Folding mirrors.
C – 35 mm camera.
S – Shutter.
O_3 – Guiding objective lens.
D_5 – Photoelectric guider occulting disk and photocells.

Fig. 12. Schematic drawing of the HAO balloon-borne coronagraph which brought the first stratospheric coronal pictures. For the first time, a 3-disk external occultation system was also employed and, additionally, a calibration channel was incorporated (from Newkirk and Bohlin, 1965).

were believed to be responsible for a series of large recurrent geo-magnetic storms. However, today we believe that coronal holes are responsible for this kind of solar-terrestrial relationships (see Section 2), and streamers are still not well understood. A better spatial resolution was needed and, also, a better time coverage, in order to follow the evolution of streamers. Later on, the same group succeeded in flying the coronagraph at a 27-day interval, showing the first indication of what we now call the helio-sheet.

4.1.2. *The French Balloon-Borne Coronagraphic Experiments*

An externally occulted coronagraph has been developed independently in France by Dollfus *et al.* (1968). Its optical schematic is shown in Figure 13. The apodization of the

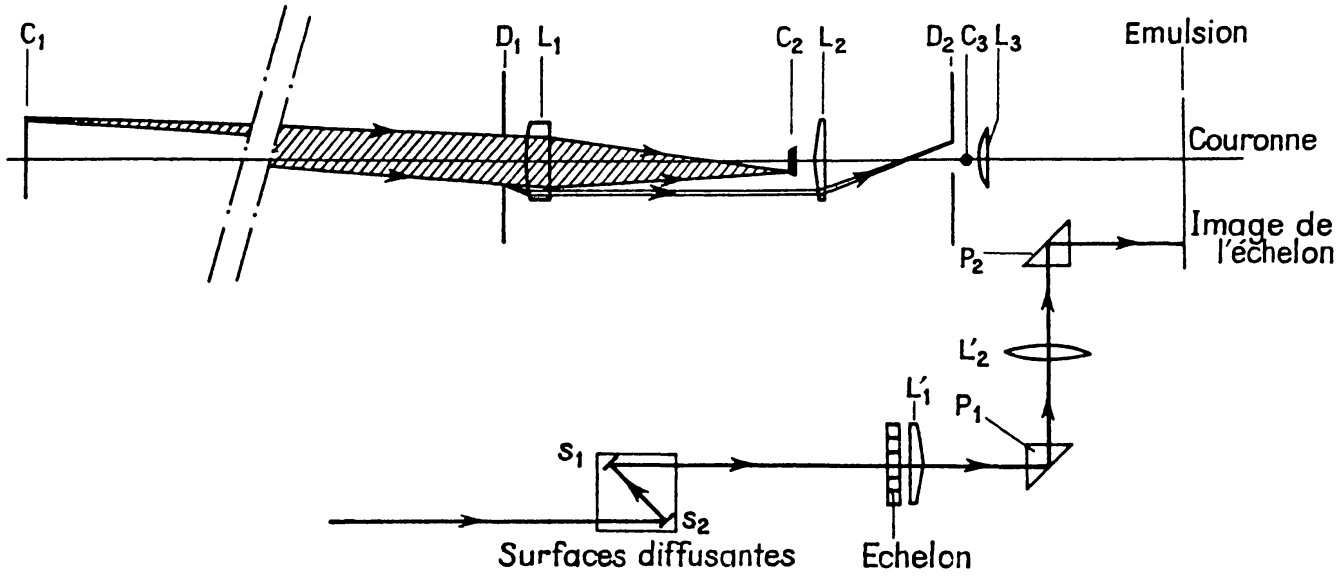

Fig. 13. Optical schematic of the French balloon-borne coronagraph (Dollfus *et al.*, 1968). The external occulting disk was serrated, with improved polishing and the Lyot scheme was properly modified to block the maximum of parasitic light.

external occulter is obtained thanks to the use of an improved serrated disk (or saw-tooth disk), proposed earlier by Purcell and Koomen (1962) and thanks to an improved inner occultation of a slightly modified Lyot scheme. Photos were made with the infra-red film Kodak-2481 and a calibration channel was also used with a step wedge. A series of flights at the CNES facilities in the south of France was performed starting in 1967 (see Figure 14), including a flight with more than five hours duration, which brought pictures with examples of transients in streamers. A more sophisticated version of this instrument, which would have included a polarimetric analysis, has been envisaged later on as a space-borne coronagraph, with a vidicon tube as a detector. Thanks to the use of the coronagraphic ground-based coverage at Pic-du-Midi Observatory around the dates of the balloon flights, and thanks also to a coordination of the dates of the flights with solar total eclipse observations, this group succeeded in

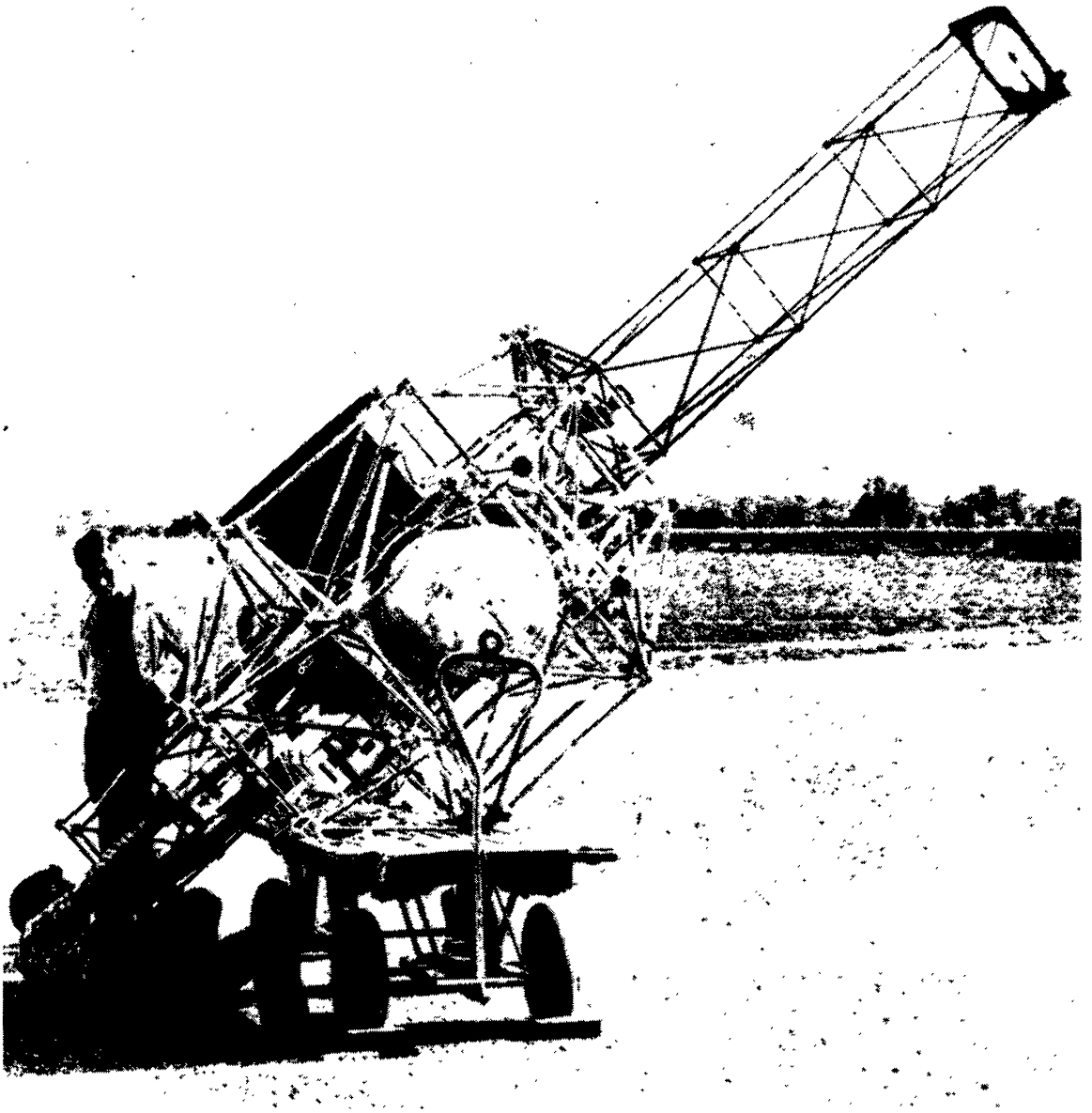

Fig. 14. The coronagraph of Figure 13 shown on the launching pad of CNES (France) before the balloon flight. A last checking of the overall alignments and a cleaning of the external disk was taking place during these last minutes (courtesy of A. Dollfus).

producing many measurements of electron densities in coronal streamers and enhancements.

4.1.3. *The Balloon-Borne Infra-Red Coronagraph*

The extension of an externally occulted coronagraph for use in the infra-red offers unique opportunities for the examination of thermal radiation of the outer corona (MacQueen, 1968a, b). This instrument is taking advantage of the wavelength dependence of the scattered light in the telluric atmosphere; the near solar sky radiance at 2200 nanometers is expected to be on the order of 6×10^{-2} times less than that of 600 nanometers, if a wavelength dependence of scattered light in the form $\lambda^{-2.2}$ is

assumed, as found by Newkirk and Eddy (1962), from their stratospheric balloon experiments (see Section 4.2.1). It is also expected that body and surface scattering produced by the primary objective will be reduced because of the δ/λ dependence, where δ is a characteristic dimension of the scattering center, although the resolution due to diffracted light is necessarily decreased as the ratio λ/r where r is the radius of the aperture of the instrument. A first generation instrument was designed and successfully flown on a balloon-borne platform in January 1967 (MacQueen, 1968). The optical schematic of the instrument is shown in Figure 15, including the description given by

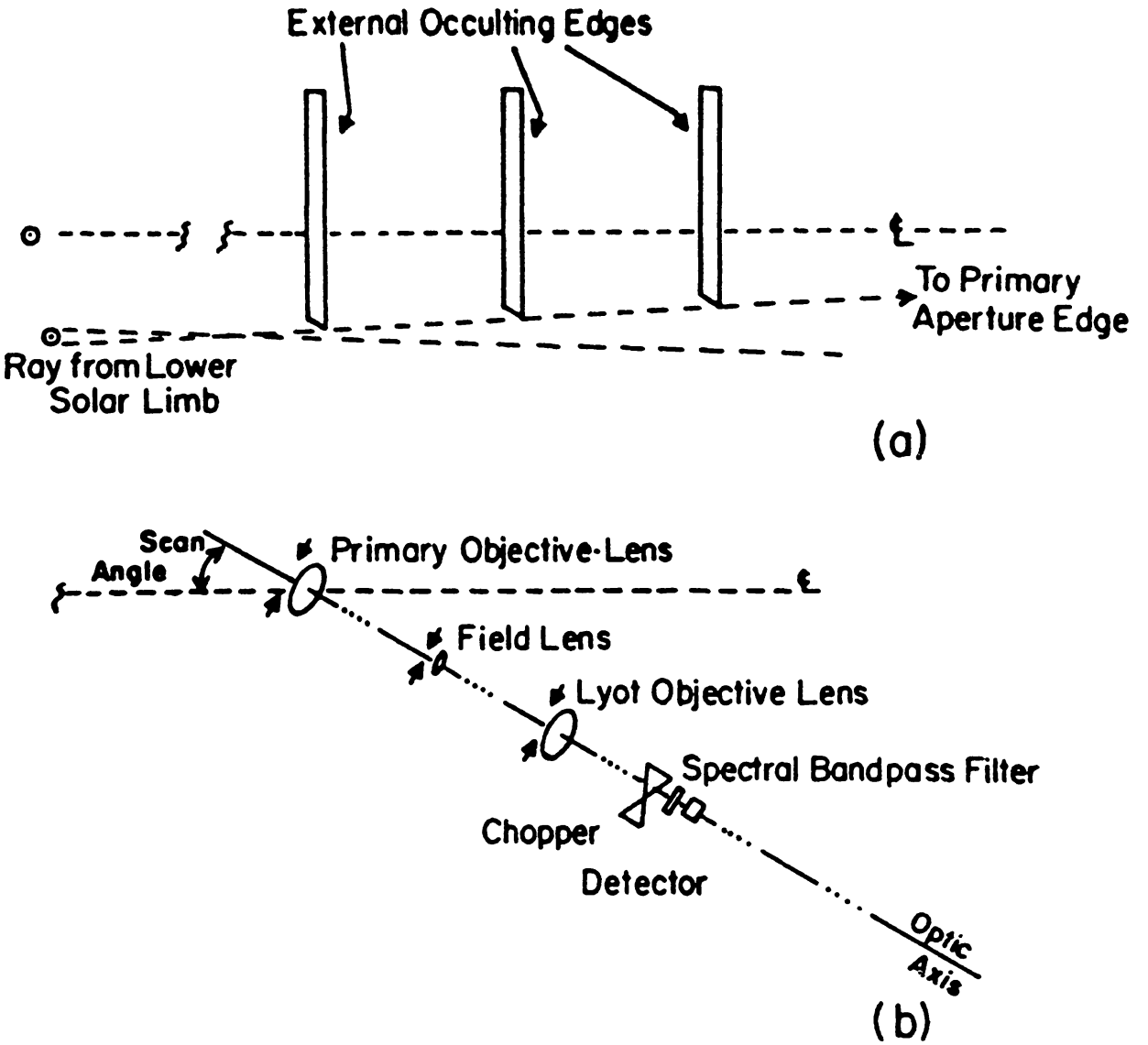

Fig. 15. Schematic diagram of the IR-balloon-borne coronagraph (after MacQueen, 1968). (a) The triple straight edge array blocked the primary objective lens from direct photospheric light, and apodized the resultant diffracted light. The edge nearest the Sun was about 400 cm from the primary objective lens. (b) The axial Lyot section. Radial scans of the corona were accomplished through rotation of the entire section about a diameter of the primary objective lens. Internal occulting occurred at the field stop plate. Light diffracted at the primary aperture is focussed by the field lens upon the Lyot aperture. The Lyot objective lens formed the entrance window to a refrigerated chamber housing the detection unit.

MacQueen, who performed its extensive analysis; he studied successively the effects produced by the straight edge system, the stray light properties of different lenses selected as primary objective, and the infrared-scanning photometer.

Unique results were obtained during the stratospheric balloon flight employing this coronagraph, including the observation of thermal emission features at 4, 8.7, and 9.2 solar radii, over a very low background decreasing to values under 10^{-10} of the average solar disk intensity, in the outer field (see MacQueen, 1968). Additionally, an equatorial enhancement was recorded beyond five solar radii at the east limb. To explain the bumps, MacQueen has proposed the effect produced by a vaporization zone which indeed was predicted earlier by several authors. However, a certain disagreement exists among observers as far as the precise position and the amplitude of the 'bumps' are concerned (see Koutchmy and Lamy, 1985). Unfortunately, there are no independent reports made recently on the topic, although two dimensional infrared detectors exist and would, presumably, now offer a better opportunity to study the infrared corona.

4.2. Rocket-borne coronagraphs

The first rocket-borne coronagraphs were designed in France (see Bonnet, 1964) and at the Naval Research Laboratory (NRL) in the U.S.A. (see Tousey, 1965). The French near-UV coronagraph failed to work at its first rocket flight from Algeria and was later abandoned, although the launching pad was moved to Guyane. The instrument used a mirror as a primary objective, but no external disk was erected to produce a shadow and the in-flight contamination by dust particles was large.

4.2.1. *The NRL Rocket-Borne Coronagraph*

The U.S. coronagraph was designed to fly on a Aerobee rocket. The rocket-borne coronagraph used a simple optical system described in Figure 16. It was designed for a ± 10 solar radii field of 32 mm diameter, recorded on 35 mm film in the final focal plane. This $f/11$ system recorded the corona quite adequately with a 2 to 5-s exposure

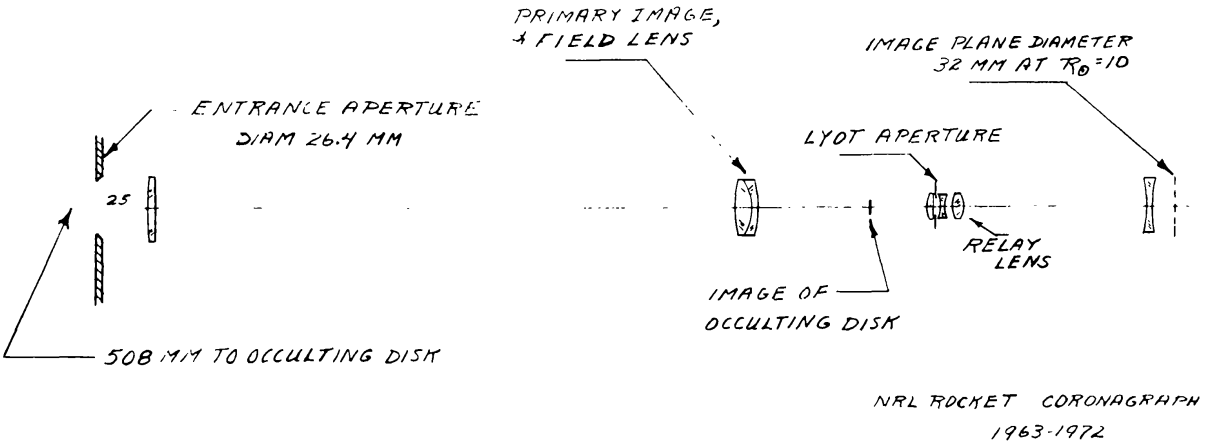

Fig. 16. Optical schematic of the first externally occulted rocket-borne coronagraph designed at NRL (Purcell and Koomen, 1962; Tousey, 1965). To make the system compact, the field lens was placed before the inner occulter.

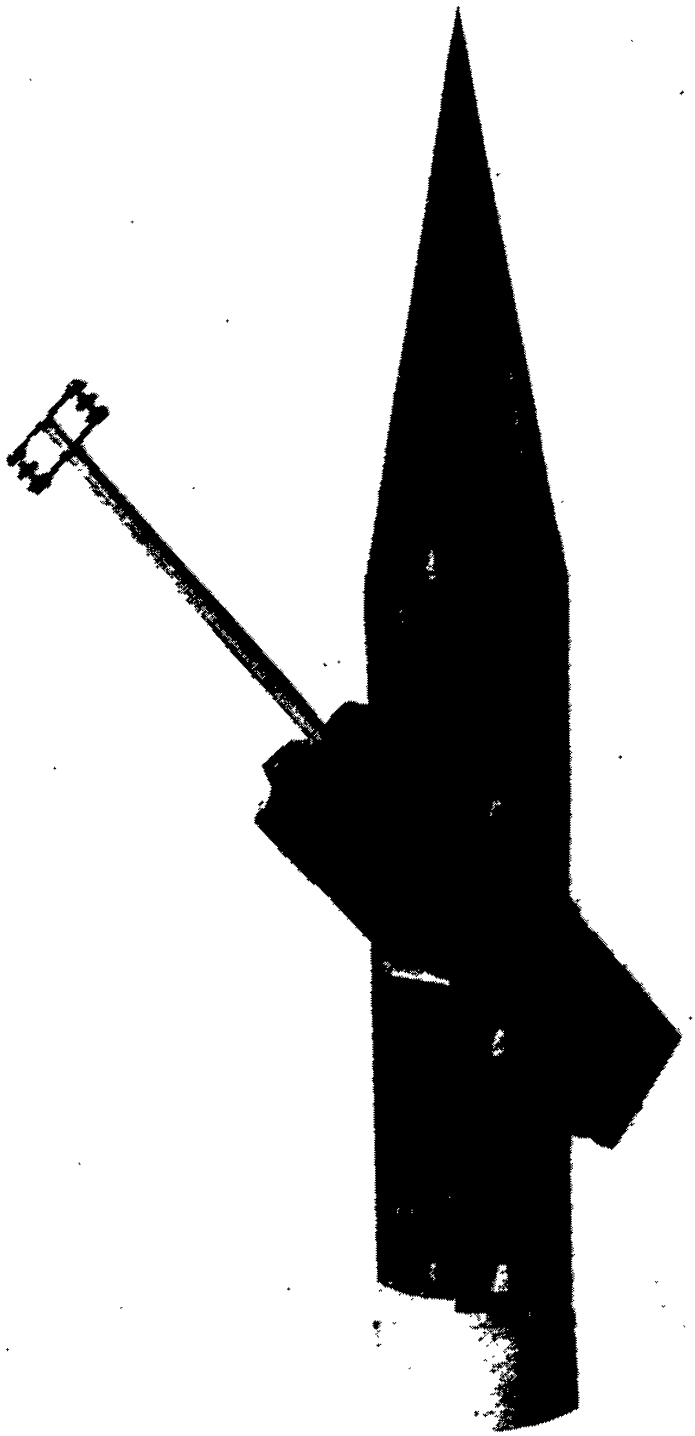

Fig. 17. The head of an Aerobee Rocket showing the NRL externally occulted coronagraphs deployed; note that a twin package was used go get simultaneously 2 images with an opposite position of the shadow produced by the pylon of the external disks.

on Kodak Spectroscopic 1-D film. No shutter was used, and the proper exposure time was the stationary interval between successive film advances. We notice that there is a true field lens of minimum diameter in the primary focal plane, and that diffracted light from the external occulting disk is not intercepted until at a point behind the field lens. Therefore, the field lens must be of coronagraphic quality. This compromise was necessary because of the severe limitations in rocket payloads (see Figure 16). The first successful flight of the system (28 June, 1963) is described by Tousey, 1965. The serrated edge occulting disk described by Purcell and Koomen, 1962, was used at first, but

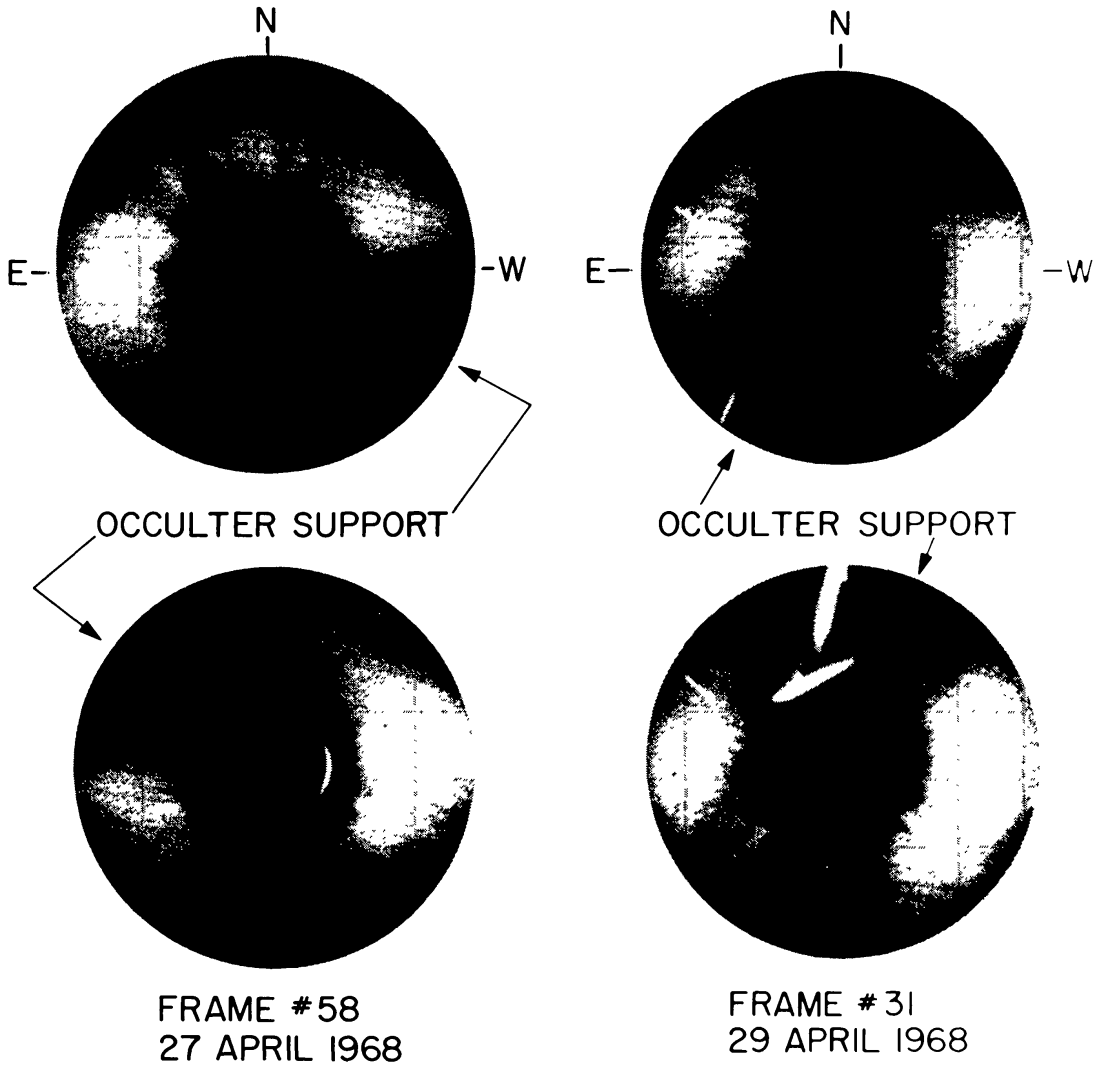

Fig. 18. Images obtained simultaneously by the rocket-borne NRL coronagraphs at 48 hours interval on April 24 and April 29, 1968. Note on the first couple of images, the disk of the Moon occulting the corona during a partial eclipse.

problems were encountered to keep the edge of each of the teeth surrounding the disk smooth and well-polished (see also Fort *et al.*, 1978). Later on, the NRL coronagraph used the 3-disk occulting system advocated by Newkirk and Bohlin, 1965. The flight rocket instrument actually consisted of two coronagraphs side by side (see Figure 17), with the occulting disks for each mounted at the end of a single spar extended between them. Thus the occulting disk supports (pylons) produced an obscuration on opposite sides so the entire corona could be reconstructed. Meanwhile, between 1963 and 1972, a dozen rocket observations were made, including two pairs of flights separated by 48 and 24 hours (see Figure 18). The same optical system was used for all these flights, but small improvements were made to reduce in-flight contamination and stray light. The generation of small particles by the rocket is one difficulty in the rocket coronagraphs. It is worth mentioning that the film plane of the rocket coronagraph usually contained a 'concentric' polarizer made by depositing the polarizing material on a rotating glass substrate. The radially polarized radiation of the electron corona is then enhanced in this part of the field and permits a correct identification of transient material in the corona, especially during the impact of a sungrazing comet which produces a huge amount of gas/dust material.

The results obtained with the NRL rocket-borne coronagraphs were described in several papers by Tousey (1965, 1973), for example. Sometimes the white-light coronagraph was operated together with XUV experiments, giving spectroheliograms of the disk and also heliograms in the band 170–500 Å (see Tousey and Koomen, 1971). The comparison of these different results brought some light on the relation between the electron corona and the monochromatic emissions, giving a good evidence of the density and temperature inhomogeneities of the corona. Because these observations were punctual, like observations during solar total eclipses, they did not show very much of

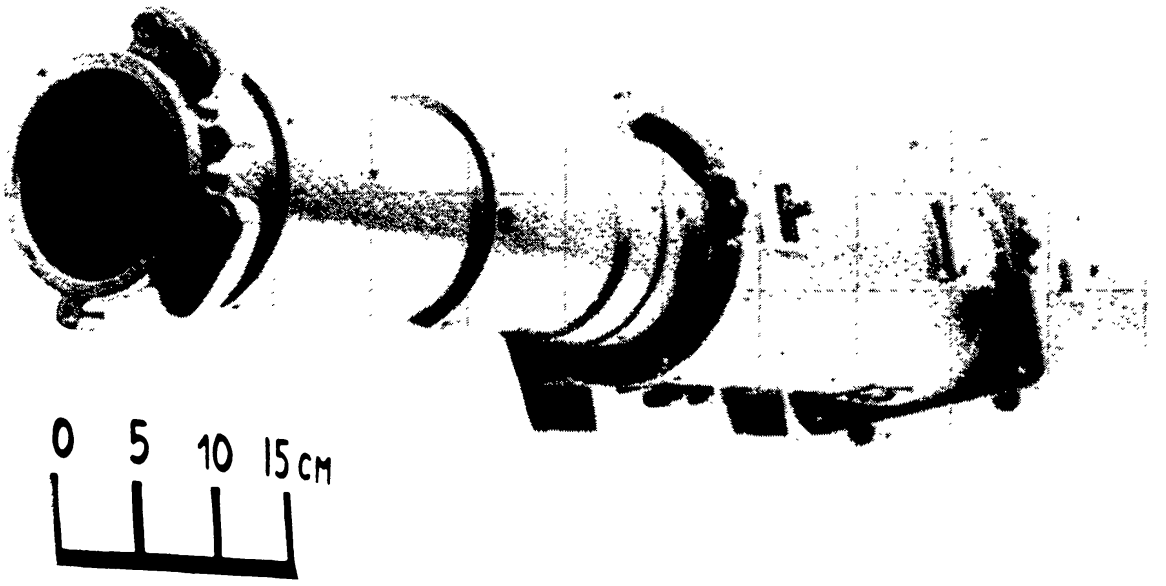

Fig. 19. The Soviet rocket-borne coronagraph (courtesy of O. Popov, Kiev Univ.). Note the importance of the baffle covering the occulting system.

the coronal dynamics. The achievement in terms of photometric precision was quite remarkable, as shown by Koomen *et al.* (1967).

4.2.2. *The Soviet Rocket-Borne Coronagraph*

Although ground-based coronography was well developed in the U.S.S.R., under the leadership of G. M. Nikolsky and others, no extensive space-borne program had been introduced to observe the solar corona. However, the Kiev University group succeeded in launching a compact rocket-borne coronagraph (see Figures 19 and 20) in December,

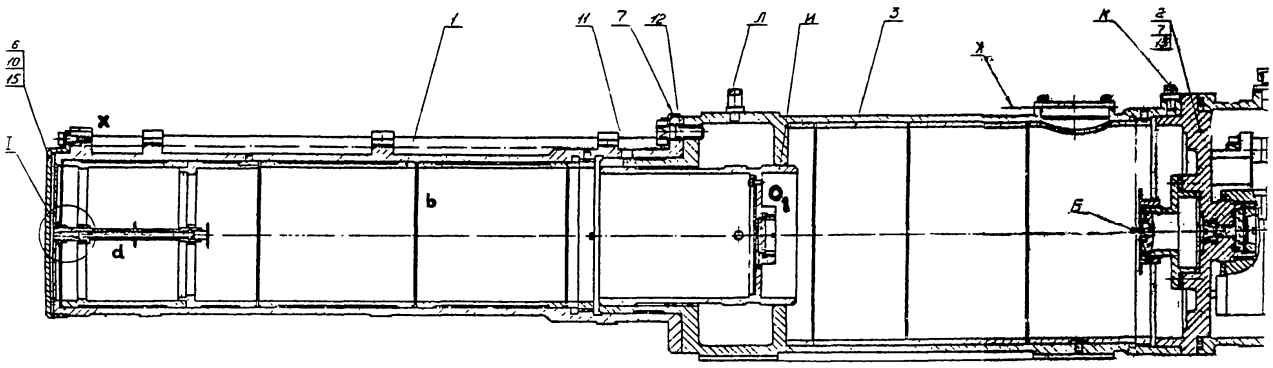

Fig. 20. Schematic drawing of the optical system of the coronagraph shown on Figure 19. O_1 is the primary objective lens. On the top, note the pin-hole X-ray miniature telescope.

1976. At the focal plane, they used a photographic camera and the absolute calibration was made on the ground using an out-focussed image of a known star. They apparently achieved a very low level of scattered light for the outer field, although a rather large baffle was used to protect the occulting system. This design seems interesting for future coronagraphs.

5. Satellite-Borne Coronagraphs

5.1. The NRL Coronagraphs

5.1.1. *The First Generation NRL Satellite-Borne Coronagraph*

The NRL rocket-borne coronagraph was redesigned to be operated on the OSO three-axis stabilized spacecraft (see Figure 21). The first attempt was made on the OSO-2 satellite in 1965. This was a *photoelectric* system behind an optical system similar to the one shown in Figure 16; the coronal image was scanned by a small aperture which was part of a rather complex mechanism producing a spiral scan. Because of high detector noise, and the primitive facilities for image processing at the time, the experiment was only a limited success.

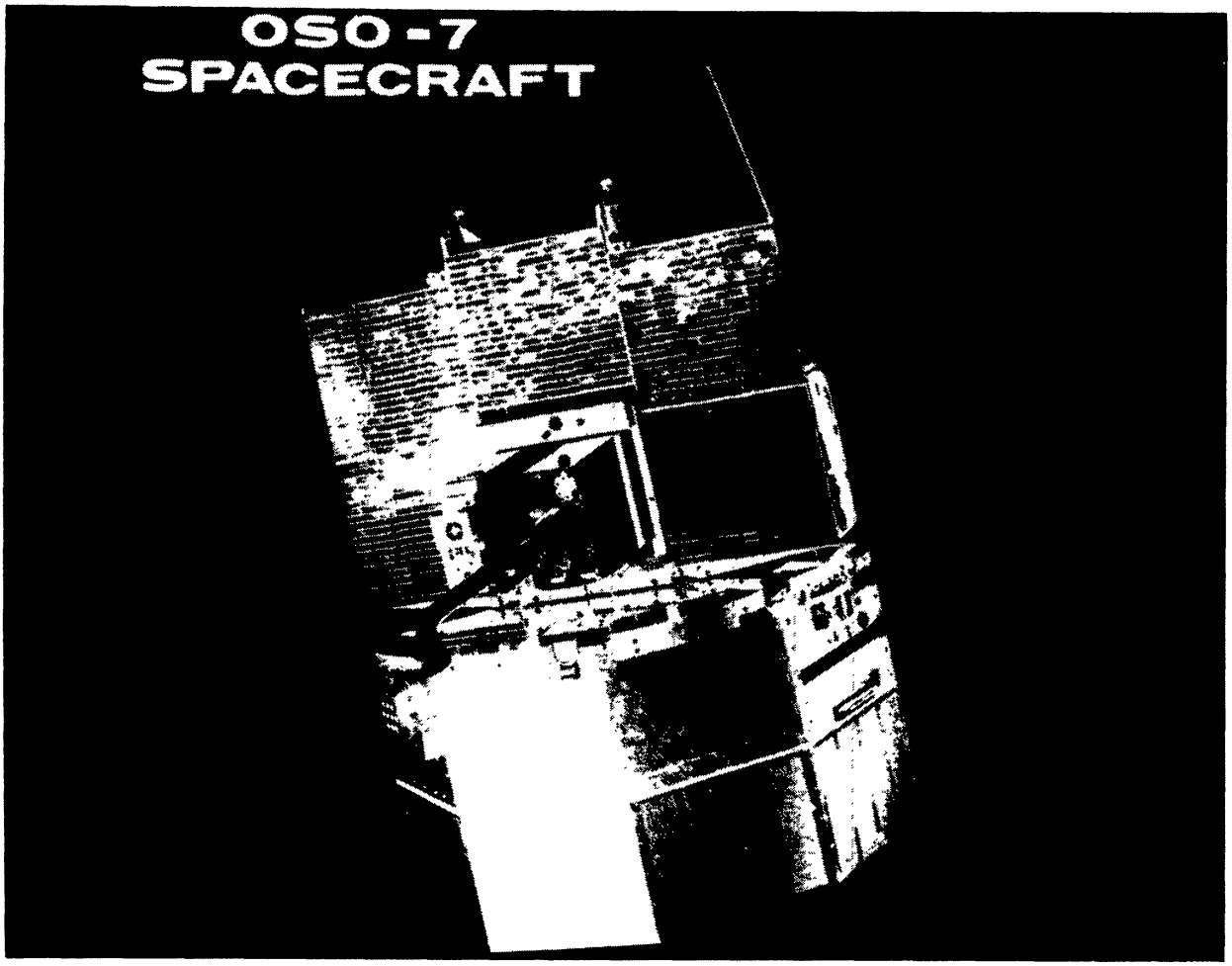

Fig. 21. The three axis stabilized spacecraft, OSO-7 with the NRL externally occulted coronagraph on it. This first satellite-borne coronagraph operating on a regular basis started the observations on October 1971 and provided day to day recording of the corona until June of 1974 (NASA photograph).

5.1.2. *The Second Generation NRL Satellite-Borne Coronagraph on OSO-7*

The first coronagraph which was operating on a regular basis, providing day to day recording of the corona, has been orbiting on the OSO-7 spacecraft from October 1971 until June 1974. Its optical system, detector package, and installation in the spacecraft has been well-described by Koomen *et al.* (1975). We show in Figure 22 the optical schematic of this elaborated instrument, which has brought a great quantity of new data. We notice that an over-occultation is chosen for this compact instrument, extending the useful field of view from 2.8 to 10 solar radii. The level of instrumentally scattered light was carefully limited, although the field lens was not put at its optimum position behind the inner occulter, but rather before it, to gain space. A single lens producing a controlled amount of chromatism was used, without any coating to minimize the amount of stray light coming from the surfaces. Calibrations were provided using both largely attenuated solar light and artificial light. Polarizers were cemented to the faceplate of the SEC Vidicon, which provided a 256 × 256 pixel image. Concentric polarizers with segments

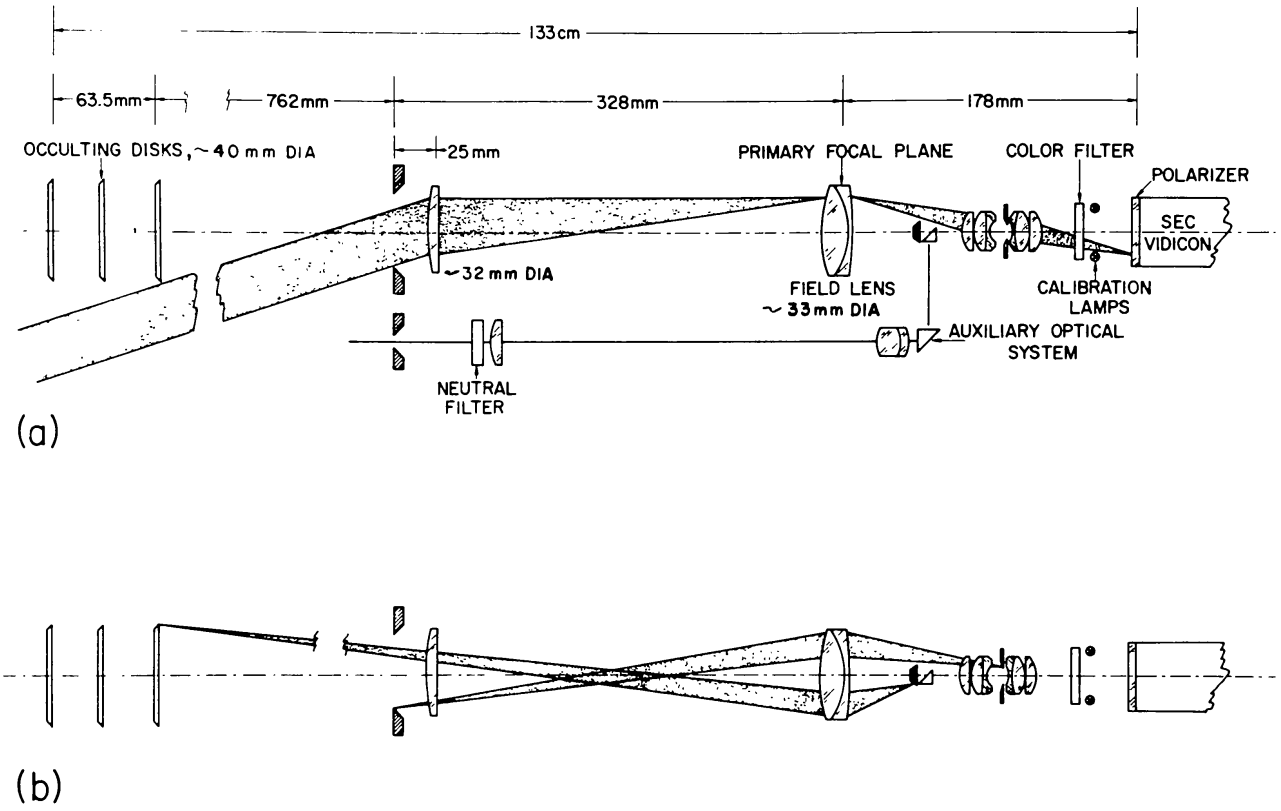

Fig. 22. Optical schematic of the NRL satellite-borne coronagraph flown on the OSO-7 spacecraft and, later on, on the P-78–1 defense satellite (SOLWIND).

of polarizing material were chosen to modulate and consequently to identify the self-radiating (non-polarized) prominence material in coronal mass ejections, or to separate the electron corona from the dust component. The detector was a Westinghouse SEC Vidicon low light-level TV camera tube working at approximately 10^{-4} lumens ft^{-2} level, so integration time in the order of two seconds was required to achieve an average signal-to-noise ratio of about 70 : 1 (8-bit digital word per pixel). Special care was taken to keep a long detector lifetime so the tube operated daily for the entire OSO-7 lifetime (October 1971–July 1974), performing more than 7000 turn-ons with little or no degradation in performance. As far as the photometric calibration is concerned, the experiment primarily addressed imaging capabilities, so only approximate intensity levels were determined. The spectral response extended from approximately 400 to 600 nanometers, so it included the H-alpha emissions. Concerning the method of observation, since the allocated recording rate for the coronagraph was slow (44 min for a full Vidicon image), alternate readout schemes were provided to record fast-changing coronal events by confining the readout sequence to any one of four picture quadrants containing the data of interest.

Figure 23 is a full field typical image recorded on January 16, 1972 during a transit of the moon over the coronal field; it illustrates quite well the main features recorded with this coronagraph: the shadow effect produced by the occulting disks and the pylon, the modulation of the coronal background produced by the polarizing 'ring' near 5 solar

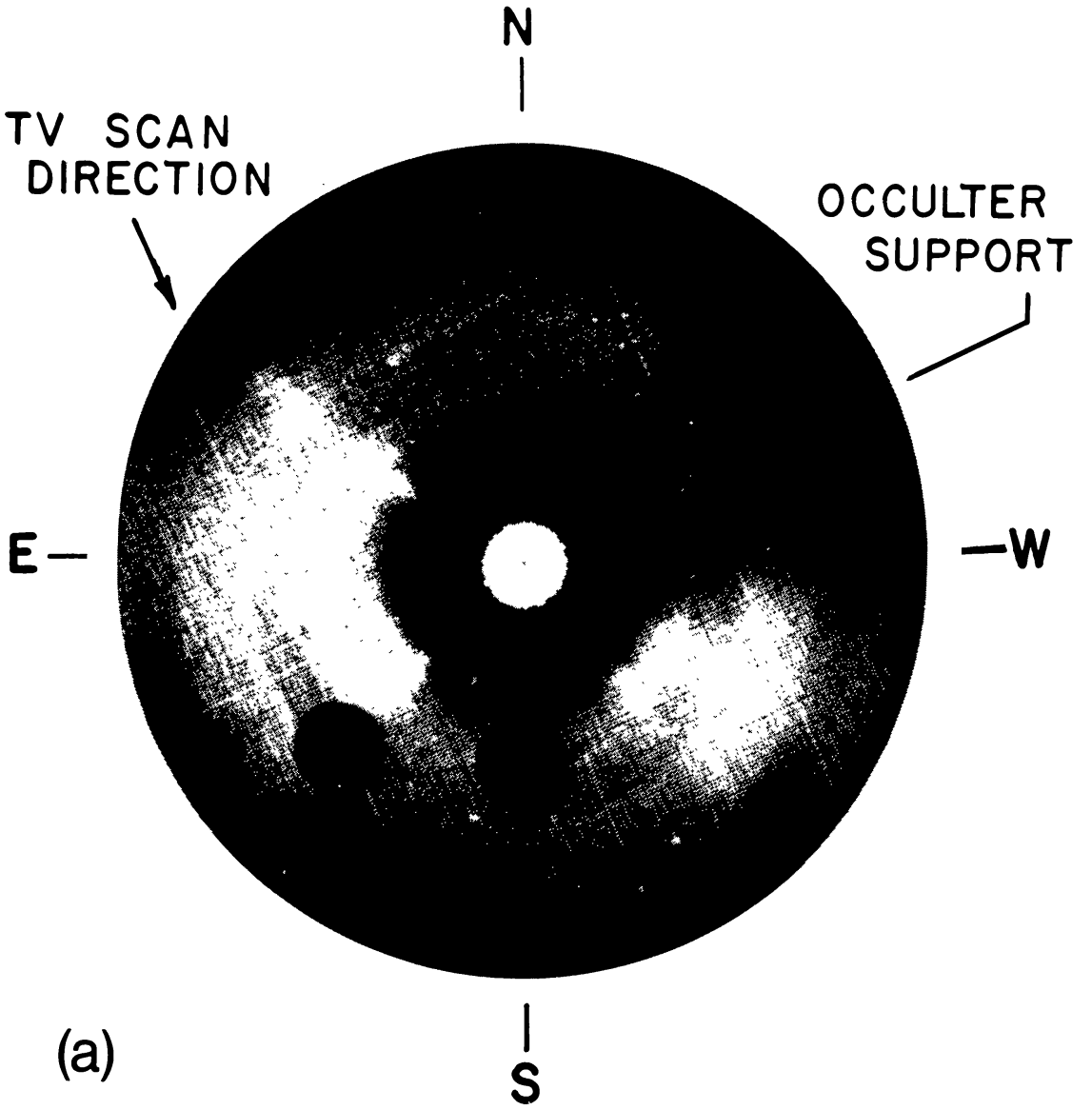

Fig. 23. Full field picture of the corona on January 16, 1972, observed with the NRL space-borne coronagraph on board of OSO-7. Note the dark concentric areas produced by the annular polarizing segments showing that the coronal streamers are strongly polarized. The Earth-lit Moon is imaged in this double-exposure sequence as it passes across the coronagraph field (courtesy of M. J. Koomen). The white disk at the center matches the solar disk.

radii, the TV-lines, etc. In Figure 24 we reproduce one of the most spectacular events recorded with this coronagraph (see Tousey, 1973). This observation is probably the first well-documented space observation of a large post-flare coronal event with mass ejection, including some amount of not fully-ionized material producing emission in 'cool' lines like H-alpha. It is really impressive as moving clouds can be easily identified with proper motion of typically 1000 km s^{-1} up to a distance in the order of 10 solar radii. More examples of transient observations are given in subsequent papers by this group (e.g., Koomen *et al.*, 1974). Therefore, the NRL coronagraph appeared to be very

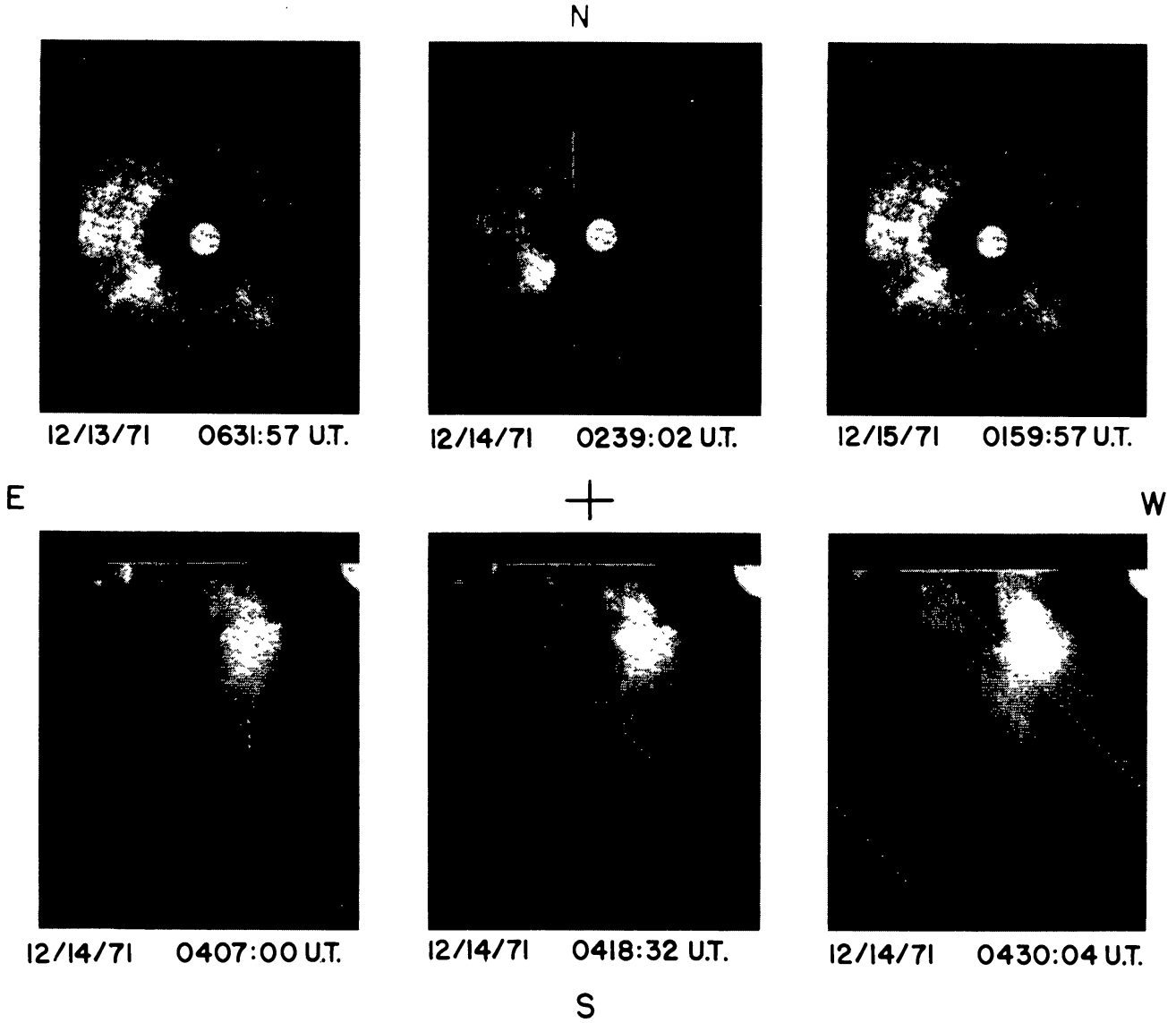

Fig. 24. Explosive-like event seen in the white-light corona following a flare which occurred behind the E-limb at about 02:39 UT on December 14, 1971, as recorded with the NRL-coronagraph on OSO-7. The three upper full-corona images show the SE-streamer before, nearly at the start of, and after the flare; its disruption began in the central picture. At this time the quadrant of interest was transmitted only by at intervals 11 min apart and produced the three lower photographs. Bright plasma clouds at the upper left of these pictures are moving outward at approximately 1000 km s^{-1}. The field is covered by a polarizer which admits tangentially polarized light (electric-vector) except for the annular bands concentric with the Sun at 5 solar radii, where the admitted vector is essentially radial. The true size of the solar disk is shown as a white disk (courtesy of M. J. Koomen).

well adapted to the qualitative analysis of mass ejection phenomena and further observations were expected.

5.1.3. *The Solwind NRL Coronagraph*

The new NRL coronagraph, called 'Solwind', was launched on February 1979 on the U.S. Department of Defense Space Test Program Satellite P78–1 (see Sheeley *et al.*, 1980). The P78–1 instrument was actually the 'flight spare' remaining from the OSO-7

flight and was identical (except for some electronics) to the instrument flown on OSO-7 (see Section 5.1.2); it has also greatly improved data and storage capabilities. It recorded coronal images from March 28, 1979 to September 13, 1985 (the satellite was destroyed as a result of a unique test of an SDI weapon), usually at 10 min intervals, during the approximately one hour sunlit portion of each 90-min near-polar orbit (see Sheeley *et al.*, 1980). With such excellent coverage, a great many coronal mass ejections (approximately 1000 events) were recorded (see Howard *et al.*, 1985 and 1986) and it was possible to determine some of their statistical properties (see also in Marsden, 1986, pp. 107–111). Figure 25 shows probably one of the most impressive sequences of a large

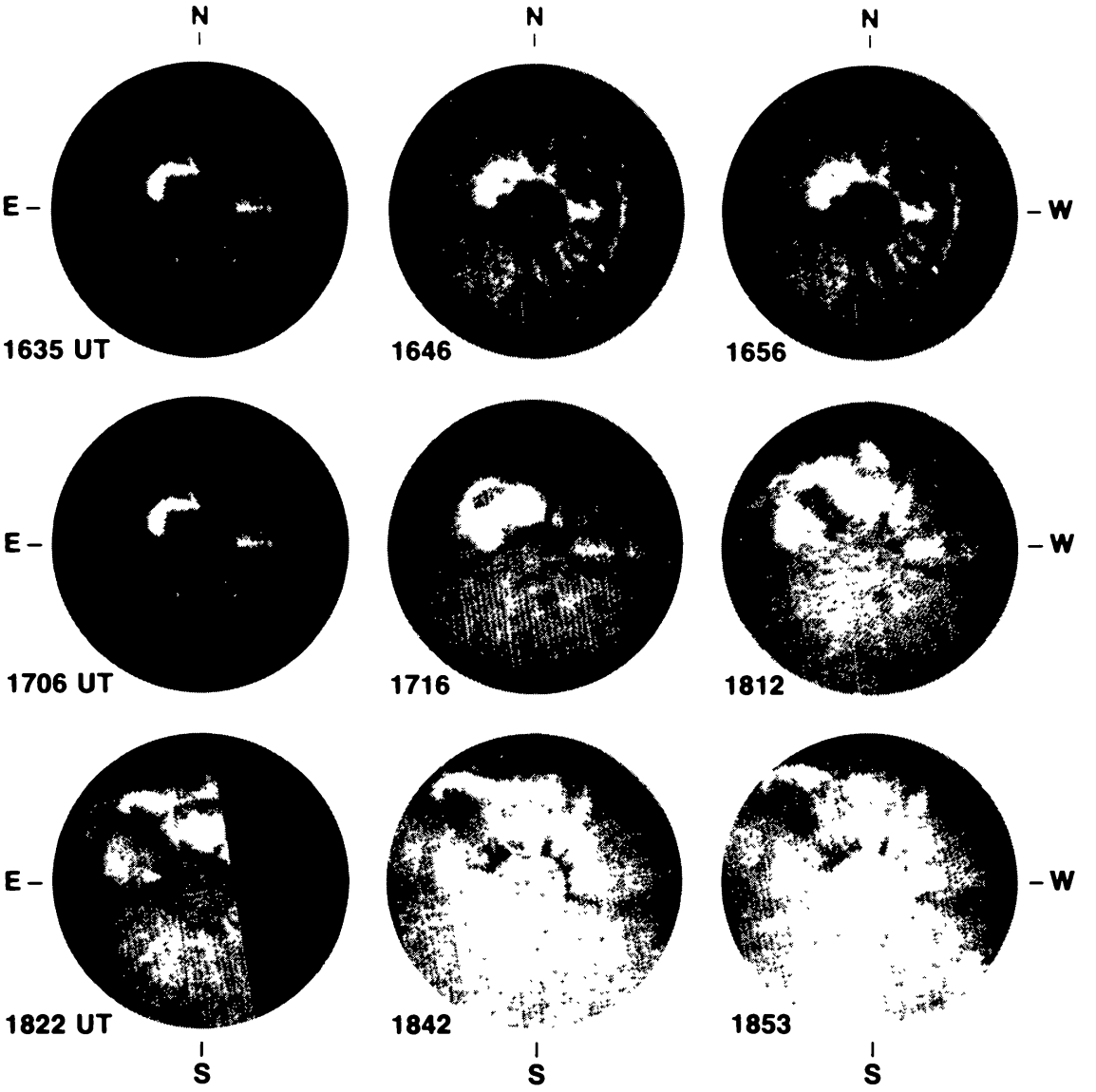

Fig. 25. A sequence of difference images from the SOLWIND coronagraph (P-78–1) showing a large coronal mass ejection observed on May 24, 1979. Note the huge loop of fully ionized coronal plasma accelerating at more than twice the rate of the cooler prominence ejecta expanding behind it, and departing the field of view at 10 solar radii with speed near 2000 km s^{-1}. The prominence expanded in size by an order of magnitude as it traversed the coronagraph's 2.5–10 solar radii field of view and its intensity was not reduced by the polarization analyzer rings. In the lower right image, the white area indicates the size of the solar disk (NRL photograph).

mass ejection observed near the sunspot maximum of activity. A huge loop of fully ionized plasma accelerated at more than twice the rate of the cooler prominence ejecta, especially seen on images taken at 1812 and 1853 (see Figure 25). The speed of the CME reaches a value as large as 2000 km s^{-1}, which is rather unusual. The prominence ejecta expanded in size by an order of magnitude during the ascent. Compared to images shown on Figure 24, these images are of better quality, in part, because a new *image processing* was introduced at the time of the Solwind observations: the use of difference images. Each difference image shows the change that has occurred between a reference image taken at the beginning of the time sequence, when the event was not still there, and a new image showing the event in progress. This method permits an increase in the contrast of the feature to be studied and a subtraction of the stationary, but spatially variable, background, including the region dominated by the effect of the shadow of the external pylon.

Observations of coronal structures taken with SOLWIND during the sunspot maximum in 1979–1981 have been described by Sheeley *et al.* (1982); at least two transients per day were recorded and quiet conditions persisted during less than 15% of the observed days. A detailed comparison of the transients observed with the SOLWIND coronagraph, and of interplanetary disturbances observed *in situ* from spacecraft, including Helios 1 and 2, has been performed by Schwenn (1986). He found increasing evidence for a three-dimensional bubble or cloud-like structure in CMEs. In several cases, CMEs directed toward the Earth (or away from it) were identified, as their outer fronts emerged on all sides of the coronagraph's occulting disk. However, the detailed sequence of events during the generation of CME was still found unclear, essentially because the lack of observations in the 1 to 2.5 solar radii region where the generation and acceleration of the CMEs are taking place.

An unintended result of the SOLWIND coronagraphic observations has been the discovery of several Sun-grazing comets on collision course with the Sun (see Michels *et al.*, 1982). The first comet discovered in the field of SOLWIND in August 30, 1979, was also the brightest. Michels *et al.* (1982) carefully studied the event and the comet was identified as being one of the group of Kreutz sungrazers with a perihelion distance of less than 1 solar radius. Accordingly, the cometary nucleus encountered dense regions of the solar atmosphere and was completely vaporized, producing a huge cloud of cometary debris and of vaporized and sublimized products. This caused a brightening of the corona over one solar hemisphere and to heliocentric distances of 5 to 10 solar radii. Two more events were still reported, leading the NRL group to suspect that sungrazers are much more common than was previously assumed. We notice that even the relatively bright comet reported in 1979 was not recorded by cometary ground-based observers. Many similar faint objects would clearly be left unobserved were it not for coronagraphic methods. Figure 26 shows a sequence of SOLWIND photos obtained on January 1981 with the image of a small cometary object identified as a small sungrazer which, evidently, either hit the Sun or was destroyed in a close encounter. We can speculate on the importance of this 'cometary' activity of the solar corona, noticing for example, that such activity could modify our view of the dust component of the

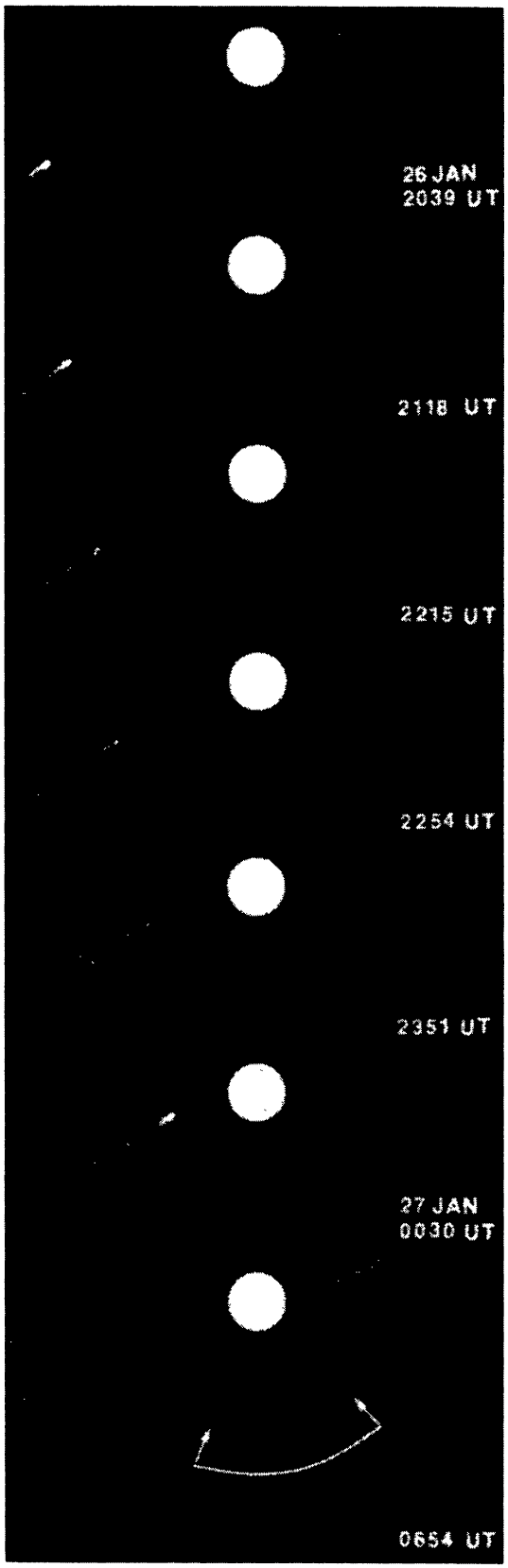

Fig. 26. Coronagraph difference images of a sungrazing comet observed on January 26 and 27, 1981 by the NRL-coronagraph SOLWIND (P-78–1). Variations in the brightness of the coma are easily discernible during the approach of the comet to perihelion. At the bottom, the arrows indicate a region in the corona through which the comet would have passed, had it survived perihelion, but no vestige of the coma was observed (NRL photograph).

corona; the products of cometary destruction should fill the space around the Sun left empty by interplanetary dust (see Section 2.3). A large infrared emission should also be present during and after these events. Future coronagraphic experiments will address these questions and even more in the field of plasma-dust interactions.

5.2. The HAO Coronagraphs

The design of the HAO satellite-borne coronagraphs, beginning with the ATM white-light coronagraph, was a natural evolution of the balloon-borne instruments flown in the sixties. Accordingly, they are well designed as far as the spatial resolution and the intensity calibration are concerned. They are also larger in size, so they require a larger platform. Therefore, the Skylab mission with its ATM module was ideal for flying such a coronagraph.

5.2.1. *The HAO White-Light Coronagraph Experiment for the Apollo Telescope Mount*

The optical system of the coronagraph is described in Figure 27, and the layout of the instrument in Figure 28. The instrument and its performance is described in MacQueen *et al.* (1974). New systems were incorporated for the first time in this instrument, namely:

(a) A pointing error system placed at the level of the primary lens O1 (see Figure 27) is employed to center the shadow of the external occulting disks around O1. At the same level, a heat-dumping mirror is used to send back the solar light entering into the light tube (Figure 28).

(b) An internal positioning system was used to maintain alignment between the internal and external occulting disks D4 and D3 in Figure 27. For this, the external occulting disk assembly has a hollow center, with an aperture concentric with the disks. Direct sunlight passes through an infrared filter of $\lambda > 750$ nanometers (the film used as a detector for these coronal studies is insensitive in this region) and illuminates the aperture. This infrared-illuminated aperture is imaged by the objective lens O1 onto the occulting disk D4 containing four silicon infrared-sensitive cells for error sensing. This permits the internal disk D4 to be servo-controlled in the right exact position.

(c) An off-axis optical path is used to produce in real time an image of a calibration wedge (matrix) on the center of each frame of film exposed. This procedure was needed as the properties of the non-linear response of the photographic emulsion in a space environment should be controlled permanently, and coronagraphic studies require at least a precise calibration. This problem has been nicely resolved with this instrument (see Poland *et al.*, 1977), and good photometric results have been reported (Csoeke-Poeckh *et al.*, 1977).

(d) An additional channel, using a SEC Vidicon TV camera as a detector, was incorporated for the visual inspection of the corona by the astronaut-crewman operating the coronagraph. Pointing and alignment were also possible, using this channel. Thanks to an extravehicular effort, the astronauts also succeeded in reducing the amount of stray light in the instrument due to particulate contamination of the first external occulting disk, by brushing it.

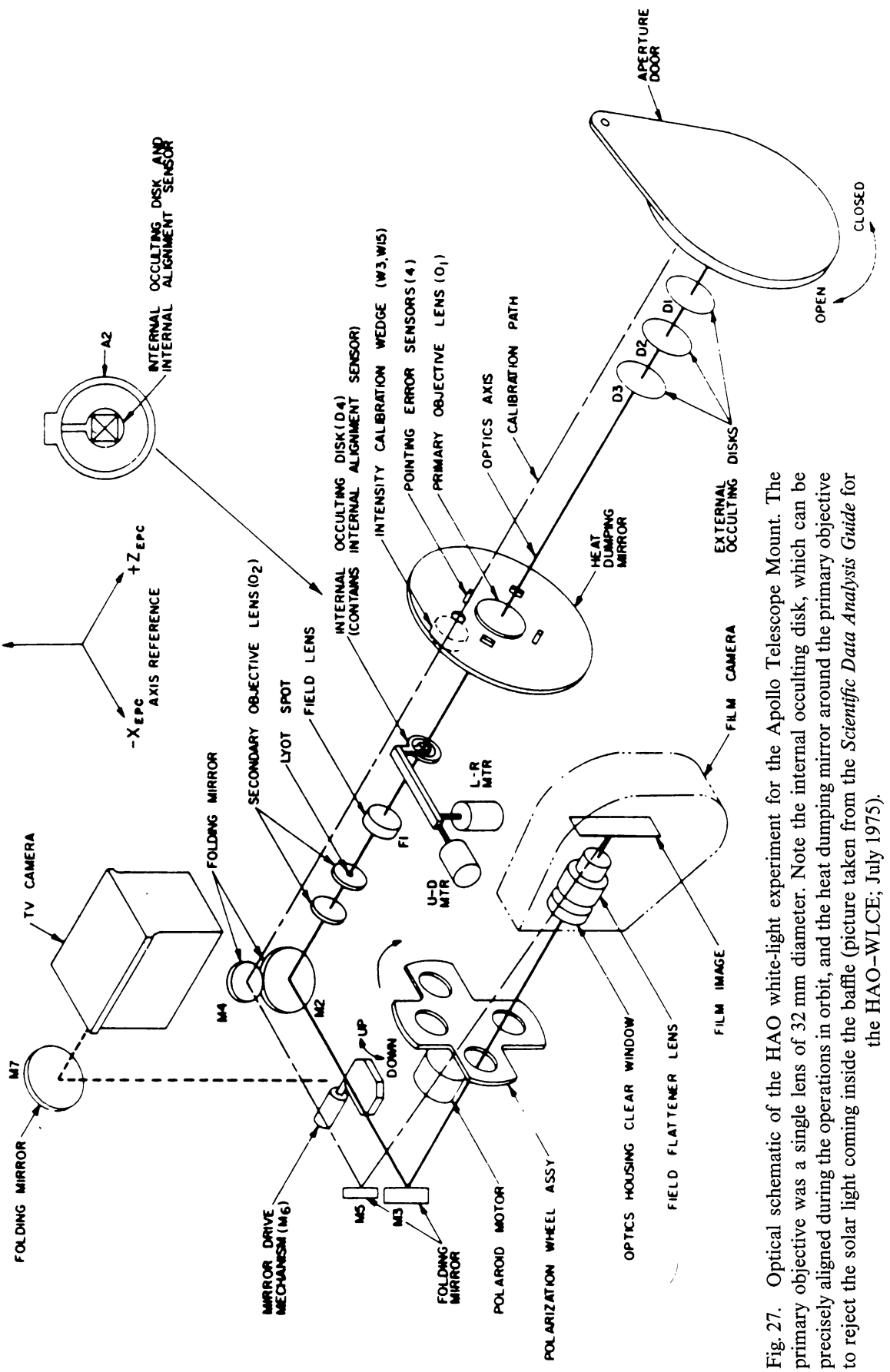

Fig. 27. Optical schematic of the HAO white-light experiment for the Apollo Telescope Mount. The primary objective was a single lens of 32 mm diameter. Note the internal occulting disk, which can be precisely aligned during the operations in orbit, and the heat dumping mirror around the primary objective to reject the solar light coming inside the baffle (picture taken from the *Scientific Data Analysis Guide* for the HAO–WLCE; July 1975).

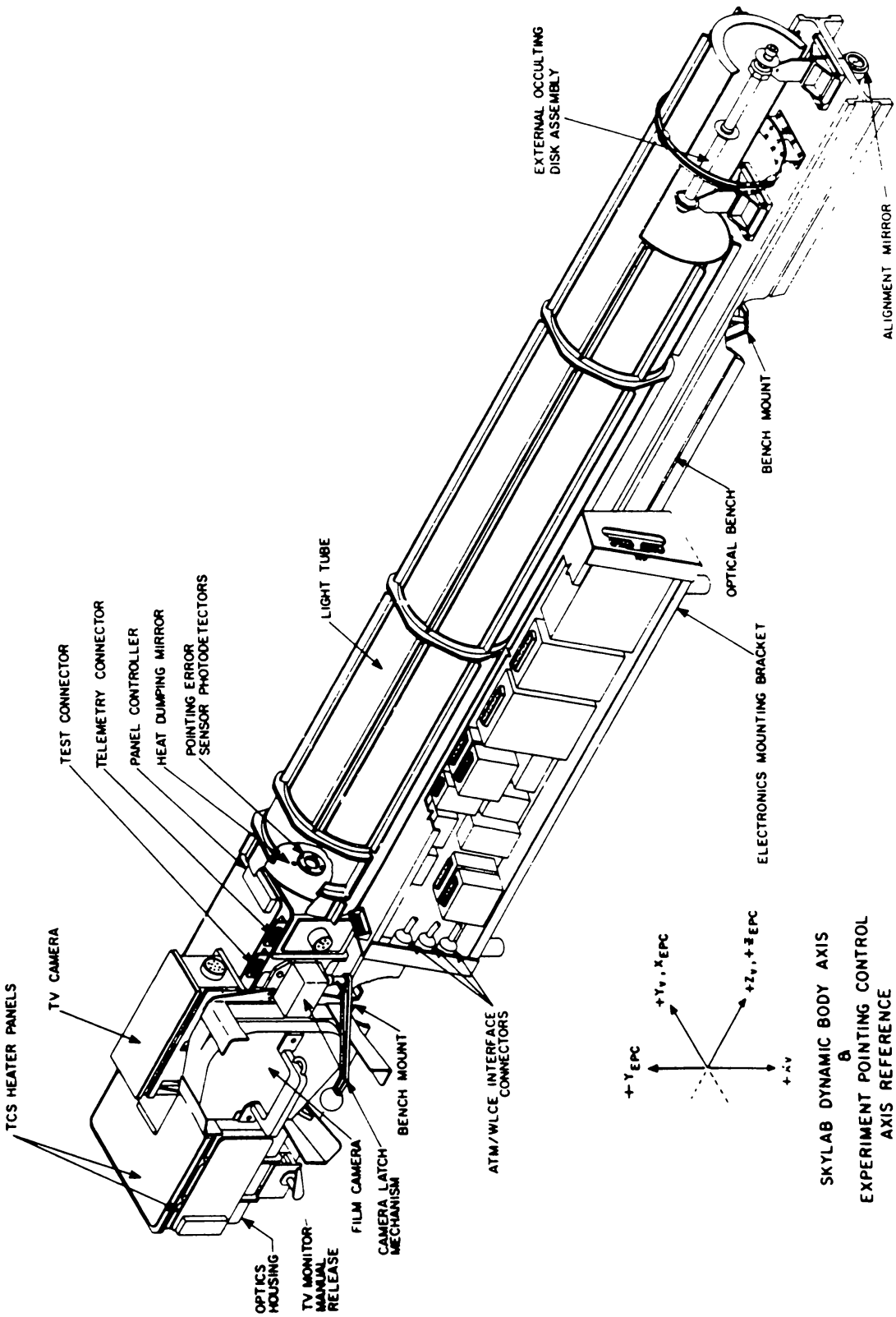

Fig. 28. Outlines of the HAO W–L coronagraph on the ATM-SkyLab Mission in 1973–1974 (the largest space-borne coronagraph ever built). Note the optical bench which was precisely pointed, taking into account the data coming from the pointing error sensor photodetectors put around the primary objective (picture taken from the *Scientific Data Analysis Guide* for the HAO–WLCE; July 1975).

A four-position wheel was also incorporated to permit observations with linear polarizers in three directions. More than 35 000 pictures were returned during the Skylab mission in 1973–74 (see MacQueen, 1980). Photos were obtained on a Panatomic-type film (see Figures 3 and 29), with exposure times on the order of 10 s. The parasitic stray

Fig. 29. Typical picture with the HAO–WLCE during the SkyLab Mission. The spatial resolution was in order of 8 arc sec at the best and the field of view extended from 1.5 to 6 solar radii. The scale on the original Panatomic-X-type emulsion was 480 arc sec per mm and images of 19 step-calibration wedge, encompassing a radiance range between 3×10^{-8} and 1×10^{-10} solar brightness was formed over the spectral range 370 to 700 nm. The instrument was capable of photographing the corona on both unpolarized and linearly polarized light. This photograph taken on December 27, 1973 shows comet Kohoutek (1973f) when it was 0.157 AU from the Sun and 1.14 AU from the Earth; the comet was behind the Sun, moving toward the left in the direction opposite to the tail and was approximately 28 hours from the perihelion (courtesy of R. MacQueen, HAO-Boulder, CO).

radiance was found to be variable in azimuth and in radial distance, the values changing from approximately 5×10^{-9} of the mean solar brightness to 3.5×10^{-10}. The main parasitic effect over the field of view was due to the shadow of the pylon (see Csoeke-Poeckh *et al.*, 1976 and Figure 29). The scientific results obtained with this instrument are extended and cover both the analysis of coronal *transients* as well as the analysis of photometric properties of the *background* corona (coronal hole; *F*-corona) (see, e.g., MacQueen, 1980; Zirker, 1977). During the 227 days of observations in a period after the sunspot maximum, 110 coronal transients were recorded. Nearly 80 transients were identified as a CME. The origins of these transients were extensively analyzed, using solar observations performed both in space and on the ground. However, a study of the relation between CMEs and other forms of solar activity is easier during the years of sunspot maximum, so a new experiment was prepared at HAO for the Solar Maximum Mission (SMM).

5.2.2. *The HAO Coronagraph/Polarimeter of SMM*

This new instrument is described by MacQueen *et al.* (1980). We extracted from the *Experiment Handbook* (E. Hildner, ed.) the layout of the experiment (see Figure 30) and the optical schematic (Figure 31). Although this coronagraph is designed for remote operations, it is rather similar to the ATM coronagraph. However, a few additional systems were incorporated which make this coronagraph the most sophisticated space-borne instrument ever flown:

(a) A sector mirror was incorporated to record with the SEC Vidicon, used as a sensor and imager, a selected quadrant of the solar corona.

(b) A doublet lens (spaced) was used as a primary objective to improve the chromatic properties of the optical train, thereby reducing the stray light in the inner field of view.

(c) Spectral filters were used to help discriminate between the electron corona and the cool gas emissions (H-alpha, etc.). Additionally, a narrow filter was incorporated to isolate the Fe XIV 530.3 nanometer emission line with the hope of measuring its polarization direction, which is believed to be related to the structure of the coronal magnetic field.

The spatial resolution of the instrument was improved over the ATM version. Pixels of 6.4 or 12.8 arc sec size and smaller fields of view than a quadrant are selectable by ground command. Figure 32 shows an example of observations made with this instrument, which is still in operation at the time of this writing. Already, many results have been published (see, e.g., MacQueen and Fisher, 1983; MacQueen *et al.*, 1986; Wagner, 1984; Hundhausen *et al.*, 1984).

Thanks to the observations performed with the C/P instrument on SMM, the CME phenomenon has received more careful attention, including small-scale effects often revealed in loop-like developing fronts. A picture of CME as an expulsion of magnetized plasma out of the gravitational potential well of the Sun has emerged. However, many questions are still open and await other precise measurements which were planned with this instrument.

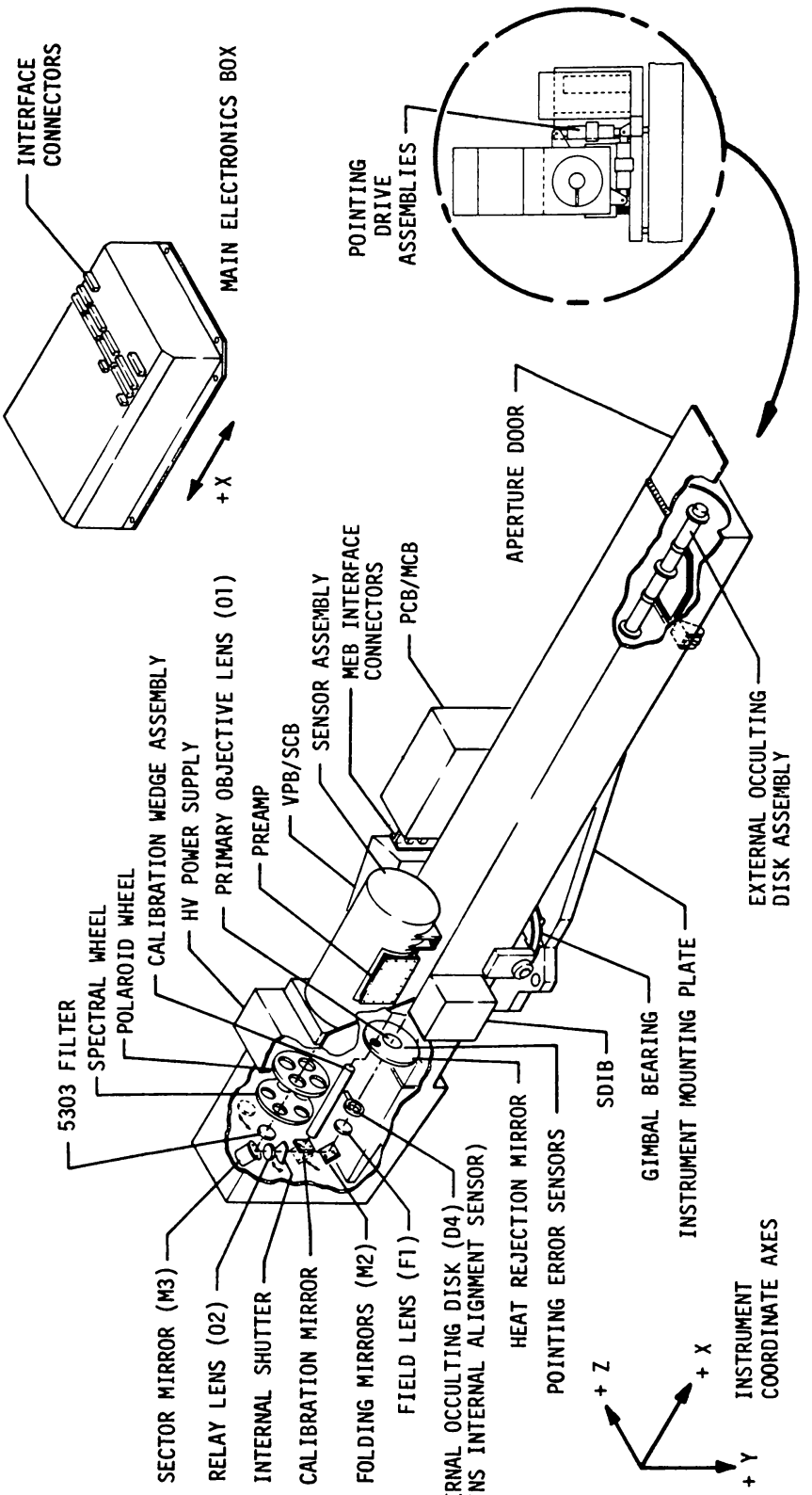

Fig. 30. Layout of the HAO Coronagraph/Polarimeter on the Solar Maximum Mission (1980). Each element and sub-system are identified on this picture taken from the *Experiment Handbook* (HAO–NCAR, E. Hildner (ed.)).

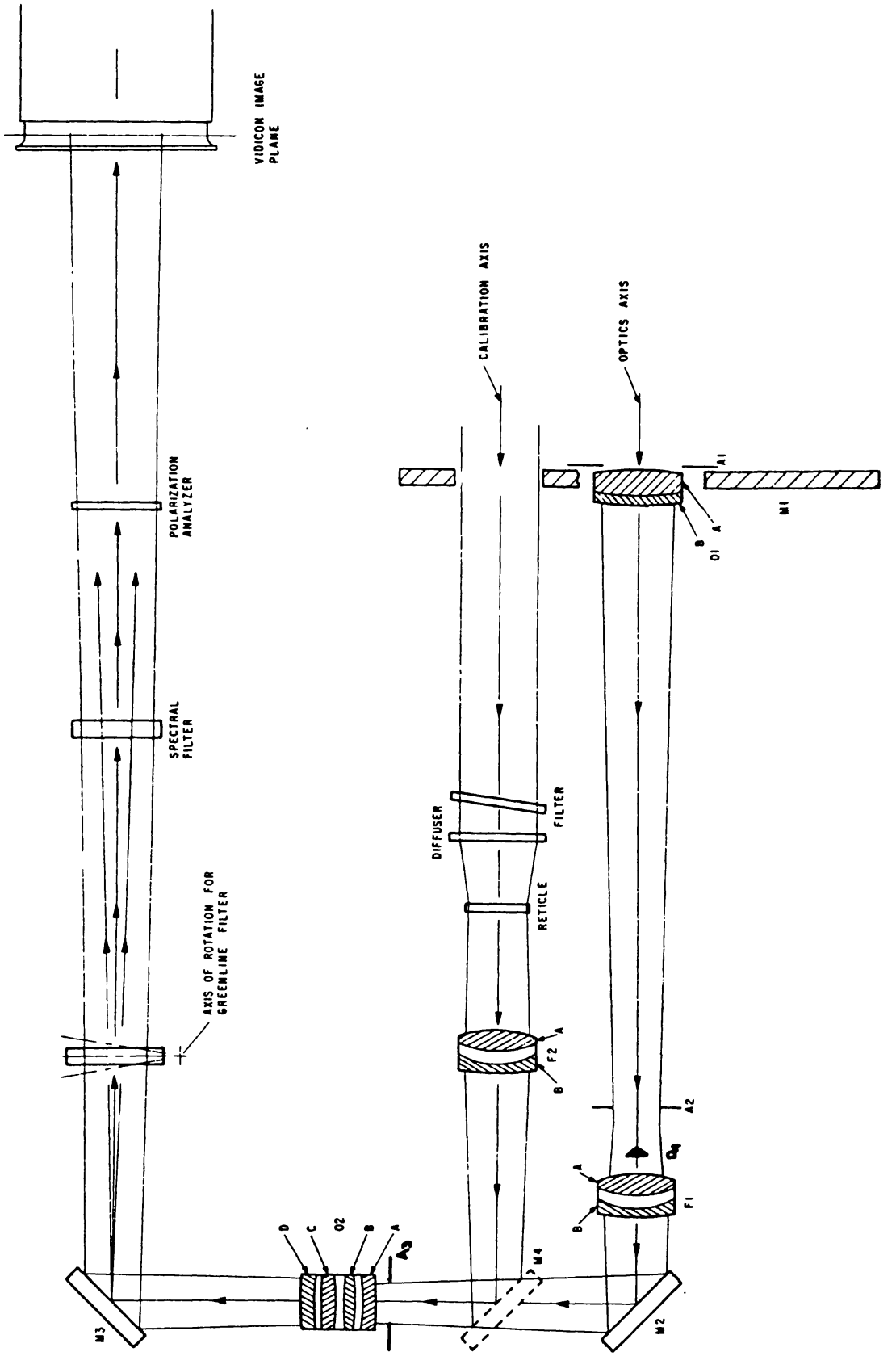

Fig. 31. Optical schematic of the HAO Coronagraph/Polarimeter on SMM. Note that a doublet spaced lens of 27 mm was used as a primary objective (from the *Experiment Handbook*; HAO–NCAR, E. Hildner (ed.)).

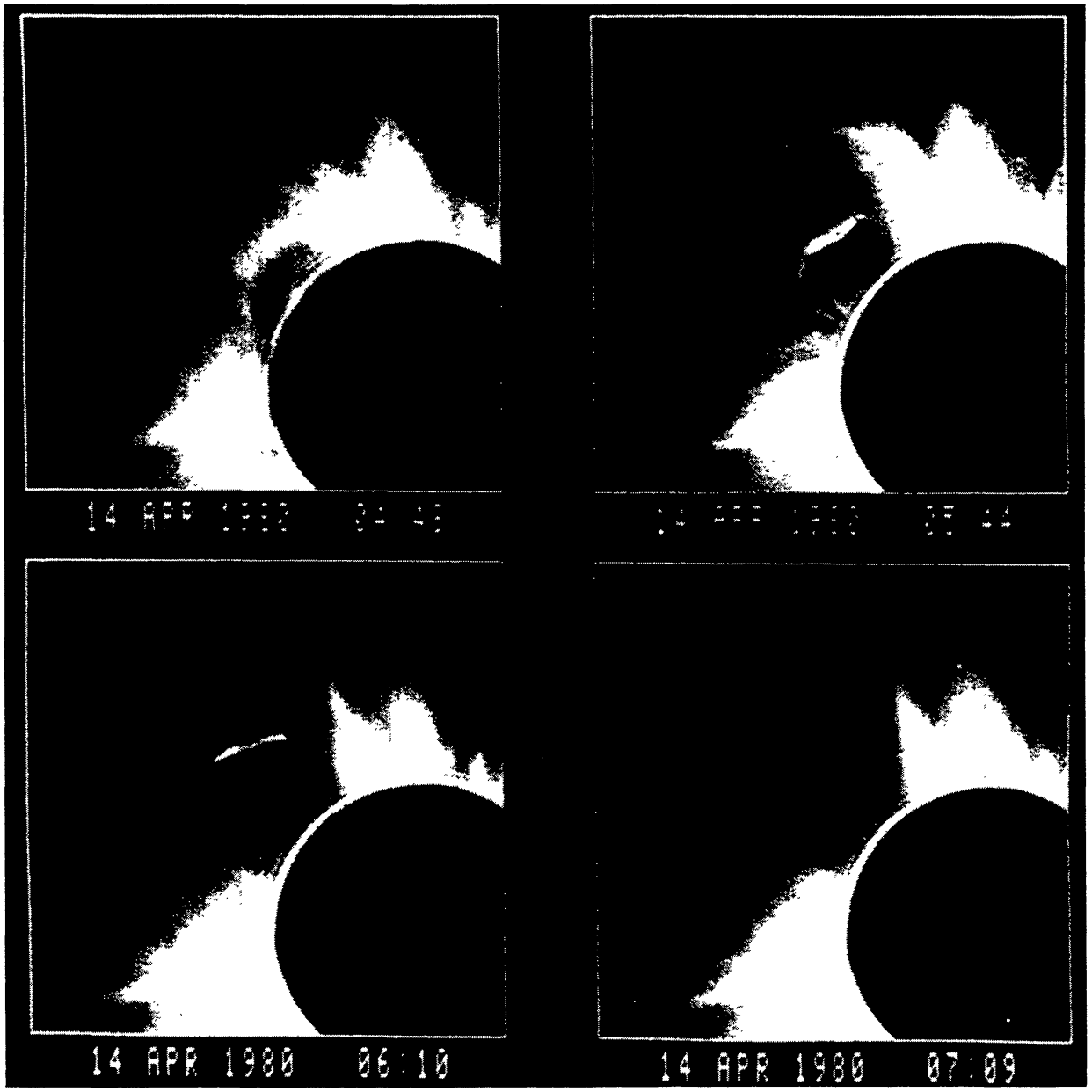

Fig. 32. Sequence of WL pictures taken with the SMM-HAO Coronagraph/Polarimeter. A large coronal mass ejection was observed, accompanied with a filament eruption (courtesy of A. Hundhausen).

5.3. Other projected space-borne coronagraphs

We now consider some significant efforts made with the aim of promoting designs of space-borne coronagraphs different from those which have been already described.

5.3.1 *The Out-of-Ecliptic Mission (I.S.P.M.) Coronagraph*

We extracted from the proposal for a 'coronagraph and X-ray/XUV telescope', in the *HAO/NCAR Executive Summary* the optical schematic shown in Figure 33 and the layout of the experiment (Figure 34). Unfortunately, the mission was abandoned, although the design is worth mentioning for the compactness and the ability to resolve the problem set by the largely variable angular size of the solar disk during the projected

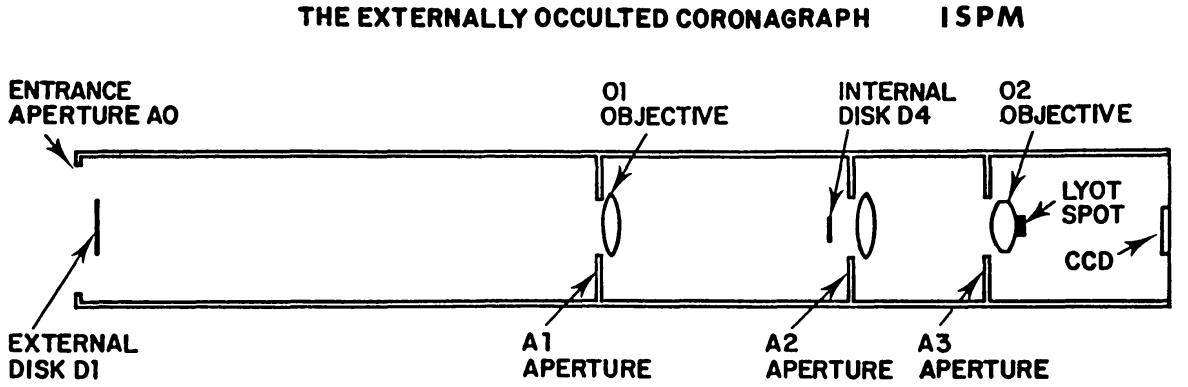

Fig. 33. Optical schematic of the projected out-of-ecliptic spacecraft (I.S.P.M.) coronagraph. The external disk was serrated and a set of 4 discrete apertures in A_1 and A_3 have to be used for different heliocentric distances. The detector was a 800 × 800 TI CCD camera (from the *ISPM-Coronagraph, X-Ray/XUV Telescope Final Report*, HAO–NCAR, 1980).

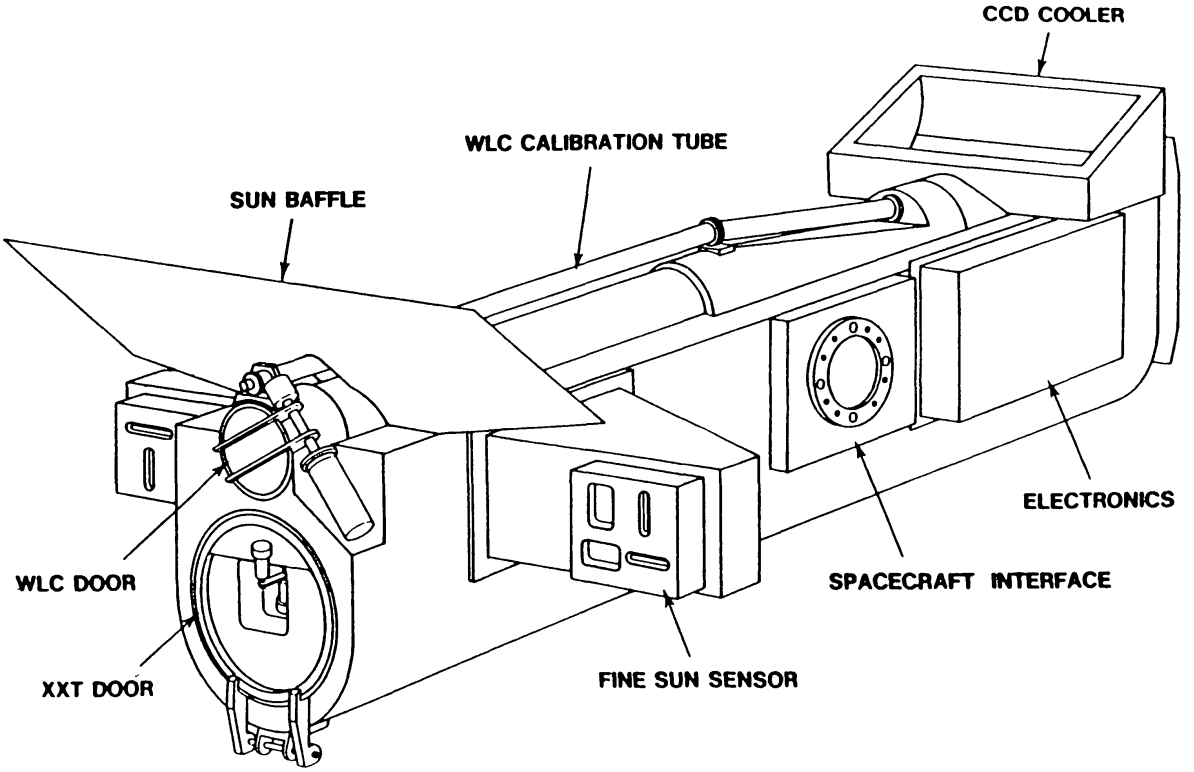

Fig. 34. As in Figure 33, but to show the layout of the whole instrument, incorporating the X-ray/XUV telescope and, above it, the W.L. coronagraph (from the *ISPM-Coronagraph, X-Ray/XUV Telescope Final Report*, HAO–NCAR, 1980).

mission (the spacecraft was to fly to Jupiter and return above the solar pole). An improved serrated disk (see Fort *et al.*, 1978) was proposed as an external occulter, and a CCD camera as a sensor-imager. The coupling of the coronagraph with an X-ray/XUV telescope would have rendered the instrument particularly efficient if the mission would not have been cancelled by NASA.

5.3.2. *The Spinning and the Scanning Coronographs*

In order to detect fainter coronal features or to produce more precise measurements, and also to perform observations in the more external regions (for example, the region outside the super-Alfvénic speed radial distance, which is estimated on average near the 15 solar radii range) of the corona, further refinements can be proposed:

(a) The level of scattered light can be greatly reduced, by a factor of approximately 100, if instead of looking simultaneously at the whole coronal field, observations are confined to a narrow sector. The diffraction light produced by a sector-like external occulter is essentially dispersed in directions outside the solid angle extended by the primary objective, giving a considerably reduced amount of stray light.

(b) The image of the whole corona is then synthesized, thanks to the rotation of the axially symmetric instrument. No azimuthal irregularity in the field is present and, a fortiori, no shadow effect produced by a pylon exists. A very small modulation ratio can then be detected.

(c) The polarization analysis can be made in precise polar coordinates with an axially rotating, symmetric coronagraph. This concept, well adapted to a spin-stabilized spacecraft, was developed for the first time by Koutchmy and Lamy (1977) and a careful theoretical treatment was given by Lensky (1981). More recently, a design was proposed (see Figure 35) for a coronagraph which is at variance to a true spinning coronagraph. In order to avoid the motion of a whole instrument when the spacecraft is three-axis stabilized, only a few light parts of the coronagraph are rotating, making this type of instrument more feasible. We hope to see one of these concepts developed in the future, quite possibly on the Space Station.

5.3.3. *Other Projects*

The HAO coronagraph has been redesigned for a joint coronagraph with the Harvard-Smithsonian Center for Astrophysics (CFA); see Kohl *et al.* (1981), to be flown with the Space Shuttle, presumably for a future spacelab mission or a 'Spartan' mission (time-limited, free-flying experiment released by the Shuttle). The CFA instrument is not a white-light coronagraph, but rather a UV coronagraph, working essentially in the Lyman-alpha region at 121.5 nanometers, with a primary mirror placed in the shadow of the entrance aperture; the instrument should then rotate around an axis pointed to the Sun, as with the spinning coronagraph described in Section 5.3.2, in order to select a coronal segment where observations are performed. Such a coronagraph is similar to the design developed in the early fifties for a UV coronagraph (see Section 4.2). However, Beckers and Argo (1983) proposed a concept for a UV coronagraph aimed to work up to Lyman-alpha with an externally occulting disk and indeed they developed such a coronagraph for a rocket-borne instrument. The Lyman-alpha flux of the corona being substantially larger than the white-light flux for a relatively 'darker' solar disk, the problem of stray light can be satisfactory resolved. Thanks to the advances gained in the super-polishing techniques of mirrors and also in coating technology, no doubt these coronagraphs will be developed for the Space Station in the near future.

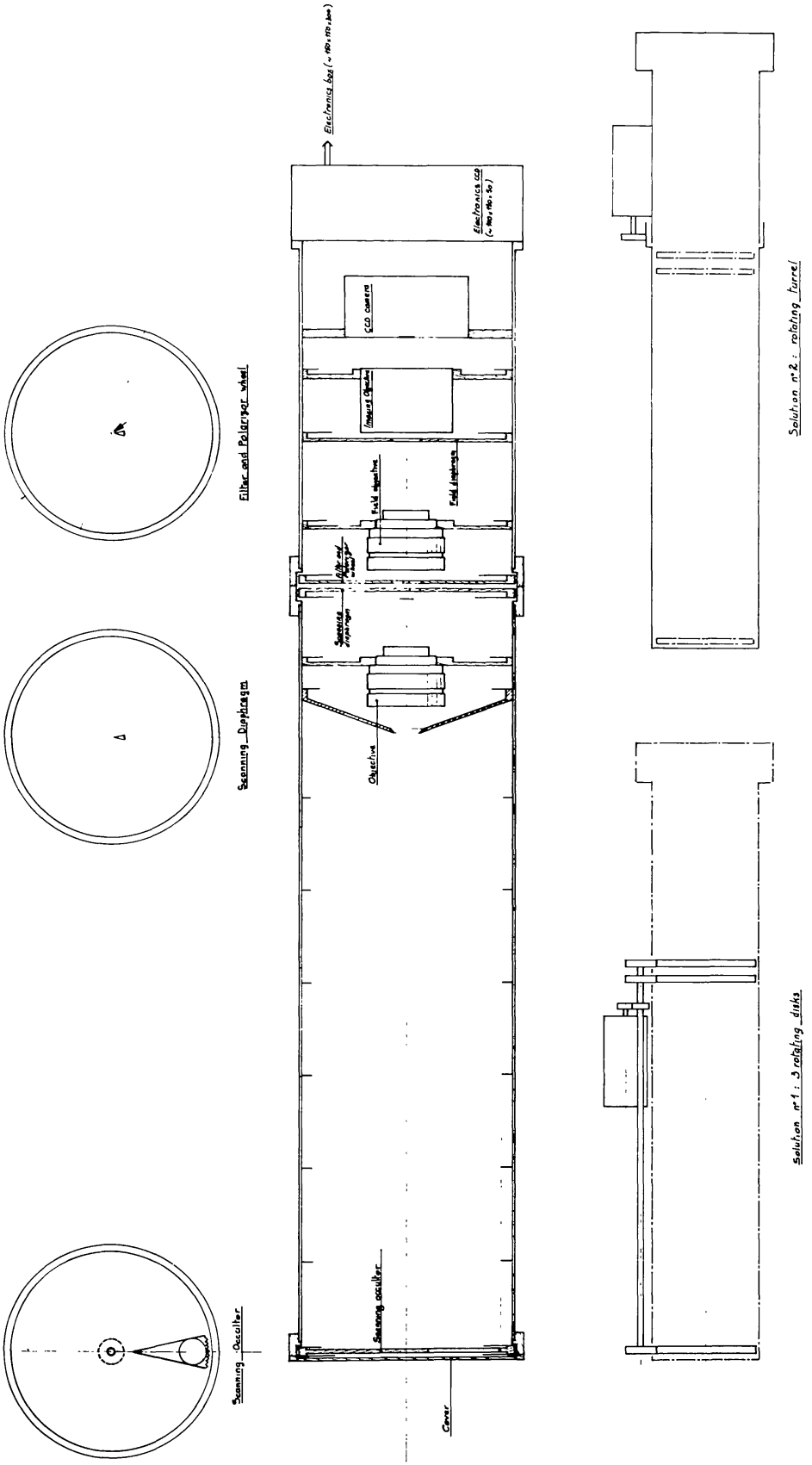

Fig. 35. Optical layout of the scanning coronagraph designed at Laboratoire d'Astronomie Spatiale-CNRS (Marseille, France) for the SOHO Spacecraft. This project has been abandoned to avoid moving parts although it presented several advantages over the classical externally occulted coronagraph (courtesy of Ph. Lamy).

6. Conclusions

Taking into account the experience accumulated in flying a dozen different coronagraphs, the critical components of such instruments can now be identified:

(a) The external occulting system (EOS, with serrated disk, triple disks, multithreads, sector, etc.) with its pylon.

(b) The primary objective (O1) with its rejection mirror (R.M.) and pointing error system (P.E.S.).

(c) The inner occulting system (IOS) with its internal alignment system (IAS).

(d) The field lens (O2) assembly, which should try also to reduce the chromatism of the instrument.

(e) The relay lens system (O3), the Lyot diaphragm (LD) and, possibly, the small inner occulters to block the stray light coming in from multiple reflections.

(f) The detector package (DP) which includes wheels with polarizers and filters.

We note that the *imaging system* (O1, O2, O3) should be achromatized as far as possible, and possess limited aberrations over the field of view, to permit a proper analysis with the DP. Furthermore, we have the *occulting and apodization* systems (EOS, IOS, LD), permitting the reduction of background stray light to satisfactory level (see Figures 1 and 5), which unfortunately reduced the performance of the imaging systems (vignetting, azimuthal non-uniformly, 'pylon' effect, etc.). Finally, additional systems should be introduced to increase the performance of the whole assembly (RM, PES, IAS...). Any future design of a new coronagraph should take each of these points into consideration as a first step. Furthermore, considerable progress should be soon reached thanks to the use of the solid-state detector arrays, like the CCD cameras which possess a large dynamic range, linear response, and high quantum efficiency. Indeed, the use of such detectors will make the inboard computer systems using multiprocessors very efficient; so we are fully confident that a whole era of coronagraphic observation is opening up, especially when observations are envisaged at the best solar site existing in the Solar System, as proposed for the SOHO spacecraft.

Many exciting new topics will be considered in the future, with the new generation coronagraphs planned for SOHO or the Space Station. This was already briefly discussed in Section 2 of this review. Let us just consider a few very specific questions which should now be addressed in new experiments:

What is the shape of coronal streamers, and how do they form and evolve?

Does a cool coronal electron gas exist, and what is its connection to prominence dynamics?

Do very short period coronal waves exist?

What is the coronal counterpart of magnetic field disturbances?

Do very high amplitude coronal magnetic fields exist?

What is the nature of coronal discontinuities and 'dark' lanes?

What is the nature of the fringes before the CME and of their forerunners?

Identification of the instability mechanisms at the origin of transient phenomena.

What is the coronal infrared radiation output during and after the encounter with a Sun-grazing comet?

What is the importance of plasma-dust interactions due to Sun-grazers of all sizes?

What is the nature of the infrared bumps, shells, and enhancements in the outer corona?

Many more questions could be added to this absolutely non-exhaustive list of actual problems, inevitably biased by the personal interest of the author. The major point here is that many essential details of solar-terrestrial physics can be understood only within the framework of coronagraphic analysis, which is the most natural way to study the circumsolar environment. Finally, this approach at the same time permits the discovery of enlightening information on the more general topic of stellar coronae, their nature, origin, and evolution.

Acknowledgements

During the course of the preparation of this review, the author greatly benefitted from discussions with Drs R. Schwenn, D. Michels, W. Wagner, M. Koomen, who especially wrote a full account of NRL coronagraphs, Ph. Lamy with whom a permanent collaboration is maintained, and R. Smartt, who manifested a constant interest. Precious documentation and encouragement were received from Dr R. MacQueen. To all of them I express my sincere thanks, as well as to J. Cornett, who helped me with the improvement of the manuscript.

References

Altrock, R. C. (ed.): 1988, *Solar and Coronal Structure and Dynamics,* 9th Sac Peak Summer Workshop, N.S.O.

Beckers, J. M. and Chipman, E.: 1974, *Solar Phys.* **34**, 151.

Beckers, J. M. and Argo, H. V.: 1983, *Proc. SPIE* **445**, 312.

Billings, D. E.: 1966, *A Guide to the Solar Corona*, Academic Press, New York.

Bonnet, R. M.: 1966, *L'Astronomie* **80**, 191.

Csoeke-Poeckh, A., MacQueen, R. M., and Poland, A. I.: 1977, *Appl. Opt.* **16**, 931.

Dolfus, A.: 1983, *L'Astronomie* **97**, 107.

Dolfus, A., Fort, B., and Morel, C.: 1968, *Compt. Rend. Acad. Sci. Paris* **266**, 1537.

Evans, J. W.: 1948, *J. Opt. Soc. Am.* **88**, 1083.

Fort, B., Morel, C., and Spaak, G.: 1978, *Astron. Astrophys.* **68**, 243.

Howard, R. A., Sheeley, N. R., Koomen, M. J., and Michels, D. J.: 1985, *J. Geophys. Res.* **90**, 8173.

Howard, R. A., Sheeley, N. R., Jr., Michels, D. J., and Loomen, M. J.: 1986, in R. G. Marsden (ed.), *The Sun and the Heliosphere in Three Dimensions*, D. Reidel Publ. Co., Dordrecht, Holland, p. 107.

Hundhausen, A. J.: 1972, *Coronal Expansion and Solar Wind*, Springer-Verlag, New York.

Hundhausen, A. J., Samyer, C. B., House, L., Illing, R. M. E., and Wagner, W. S.: 1984, *J. Geophys. Res.* **89**, 2639.

Jackson, B. V. and Hildner, E.: 1978, *Solar Phys.* **60**, 155.

Kohl, J. L., Withbroe, G. L., Wesser, H., MacQueen, R. M., and Munro, R. H.: 1981, *Space Sci. Rev.* **29**, 419.

Koomen, M. J., Detwiler, C. R., Brueckner, G. E., Cooper, H. W., and Tousey, R.: 1975, *Applied Opt.* **14**, 743.

Koomen, M. J., Howard, R. A., Hansen, R., and Hansen, S.: 1974, *Solar Phys.* **34**, 447.

Koomen, M. J., Tousey, R., and Seal, R. T., Jr.: 1967, *10th COSPAR Meeting, 'Moon and Planets ||'*, North-Holland Publ. Co., Amsterdam.

Koutchmy, S.: 1977, in A. Bruzek and C. J. Durrant (eds.), *Illustrated Glossary for Solar and Solar-Terrestrial Physics*, D. Reidel Publ. Co., Dordrecht, Holland, p. 39.

Koutchmy, S. and Belmahdi, M.: 1988, *J. Opt. (Paris)* (in press).
Koutchmy, S. and Lamy, Ph.: 1977, *Out-of-Ecliptic Mission Proposal of a Scanning Coronagraph*, NASA/ESA.
Koutchmy, S. and Lamy, Ph.: 1985, *IAU Colloq.* **85**, 63.
Lebecq, Ch., Koutchmy, S., and Stellmacher, G.: 1985, *Astron. Astrophys.* **152**, 157.
Lensky, A. V.: 1977, *Soln. Dannye* **3**, 82.
Lensky, A. V.: 1981, *Astron. Zh.* **58**, 648 (*Soviet Astron. J.* **25**, (3), 366).
Lyot, B.: 1939, *Monthly Notices Roy. Astron. Soc.* **99**, 580.
MacQueen, R. M.: 1968a, *Appl. Opt.* **7**, 1149.
MacQueen, R. M.: 1968b, *Astrophys. J.* **154**, 1059.
MacQueen, R. M.: 1980, *Phil. Trans. Roy. Soc. London* **A297**, 605.
MacQueen, R. M. and Fisher, R. R.: 1983, *Solar Phys.* **89**, 89.
MacQueen, R. M., Hundhausen, A. J., and Conover, C. W.: 1986, *J. Geophys. Res.* **91** (A1), 31.
MacQueen, R. M., Gosling, J. T., Hildner, E., Munro, R. H., Poland, A. I., and Ross, C. L.: 1974, *'Instrumentation' in Astronomy II, Proceedings S.P.I.E.* **44**, 207.
MacQueen, R. M., Csoeke-Poeckh, A., Hildner, E., House, L., Reynolds, R., Stanger, A., Tepoel, H., and Wagner, W.: 1980, *Solar Phys.* **65**, 91.
Marsden, R. G.: 1986, *The Sun and the Heliosphere in Three Dimensions*, D. Reidel Publ. Co., Dordrecht, Holland.
Michels, D. J., Sheeley, N. R., Jr., Howard, R. A., and Koomen, M. J.: 1982, *Science* **215**, 1097.
Newkirk, G. and Eddy, J.: 1962, *Sky Telesc.* **24**, 77.
Newkirk, G., Jr. and Bohlin, D.: 1963, *Appl. Opt.* **2**, 131.
Newkirk, G., Jr. and Bohlin, D. J.: 1965, *Ann. Astrophys.* **28**, 234.
Parker, E. N.: 1972, *Astrophys. J.* **174**, 499.
Pneuman, G. W.: 1986, *Space Sci. Rev.* **43**, 105.
Poland, A. I.: 1986, *Coronal and Prominence Plasmas*, NASA CO 2442.
Poland, A. I., Gosling, J. T., MacQueen, R. M., and Munro, R. H.: 1977, *Appl. Opt.* **16**, 926.
Popov, O. C.: 1980, *Astrometria i Astrofizika* **40**, 100.
Purcell, J. D. and Koomen, M. J.: 1962, *J. Opt. Soc. Am.* **52**, 596 (abstract).
Purcell, J. D. and Koomen, M. J.: 1962, in *Report of NRL Progress* (Washington), p. 9.
Rosner, R.: 1986, in Osaki (ed.), *Hydrodynamic and Magnetohydrodynamic Problems in the Sun and Stars*, Tokyo, p. 37.
Schwenn, R. R.: 1986, *Space Sci. Rev.* **44**, 139.
Schwenn, R.: 1987, private communication.
Sheeley, N. R., Jr., Michels, D. J., Howard, R. A., and Koomen, M. J.: 1980, *Astrophys. J.* **237**, L99.
Sheeley, N. R., Jr., Howard, R. A., Koomen, M. J., Michels, D. J., Harvey, K. L., and Harvey, J. W.: 1982, *Space Sci. Rev.* **33**, 219.
Smartt, R. N.: 1979, *Proc. S.P.I.E.* **190**, 58.
Tousey, R.: 1965, *Ann. Astrophys.* **28**, 600.
Tousey, R.: 1973, *Space Research XIII*, Akademie-Verlag, Berlin, p. 713.
Tousey, R. and Koomen, M. J.: 1971, *Solar Phys.* **21**, 401.
Wagner, W. J.: 1984, *Ann. Rev. Astron. Astrophys.* **22**, 267.
Zirker, J. B.: 1977, *Coronal Holes and High-Speed Wind Streams*, Colorado Ass. Univ. Press, Boulder.
Zirker, J. B.: 1985, *Solar Phys.* **100**, 281.
Zirker, J. B.: 1987, in A. Dalgarno and D. Layzer (eds.), *Spectroscopy of Astrophysical Plasmas*, Cambridge Astrophysics Series.